

Integrating genome-scale metabolic models into the prediction of microbial kinetics in natural environments

Benjamin Shapiro¹, Tori M. Hoehler², and Qusheng Jin^{1,*}

¹Department of Earth Sciences, University of Oregon, Eugene, OR 97403, USA

²NASA Ames Research Center, Mail Stop 239-4, Moffett Field, CA 94035, USA

*Corresponding author. qjin@uoregon.edu. Phone: (541) 346-4999.

Abstract

8 We propose a new method to predict microbial metabolic rates in natural environments
9 using genome-scale metabolic models. This method is a hybrid of existing approaches, i.e., rate
10 laws and flux balance analysis (FBA). It accounts for the availabilities of chemical energy and
11 growth nutrients in the environment, and applies FBA independently to the respiration and
12 biosynthesis pathways of genome-scale metabolic models. We illustrate the new method by
13 modeling the metabolism of a representative methanogen – *Methanosaarcina barkeri* – in
14 laboratory reactors and in pristine and biostimulated aquifers. The laboratory application
15 demonstrates that the hybrid method predicts the rates of individual biochemical reactions within
16 overall cell metabolism and tracks, explicitly, cellular fluxes of carbon and energy. The aquifer
17 applications reveal that the growth of methanogens in natural systems can be limited by multiple
18 factors, including energy sources and growth nutrients, and that the limitations are subject to
19 Liebig’s Law of the Minimum. These results highlight the improvements of the new method in
20 biogeochemical reaction modeling, including its applicability to diverse environments, from
21 eutrophic to oligotrophic.

22 **Keywords:** genome-scale metabolic model, biogeochemical reaction modeling, microbial
23 kinetics, flux balance analysis, nutrient limitation, methanogenesis

24 **1. Introduction**

25 Biogeochemical reaction modeling simulates, numerically, concurrent geochemical
26 reactions and microbial metabolisms in natural environments (Bethke, 2008). This method
27 combines geochemical and microbial reaction models. Geochemical models focus on chemical
28 speciation, redox reactions, mineral precipitation and dissolution, and other abiotic reactions.
29 Microbial models describe microbial reactions and the development of microbial populations. By
30 coupling microbial and geochemical models, biogeochemical reaction modeling offers a
31 quantitative assessment of microbial processes in natural environments, and has become a
32 routine tool for both theoretical and practical applications, such as element cycling and the
33 contamination and remediation of groundwater (Druhan et al., 2012; Jin and Roden, 2011;
34 Johannesson and Neumann, 2012).

35 Classical approaches simulate microbial metabolisms using black-box models (Jin et al.,
36 2013). These models bypass biochemical pathways and metabolic regulation, and compute rates
37 of respiration and growth directly from environmental concentrations of energy sources and
38 growth nutrients using rate laws (Monod, 1949; Simkins and Alexander, 1984). For example,
39 they calculate respiration rates r'_R ($\text{mol}\cdot\text{g}^{-1}\cdot\text{s}^{-1}$) using the thermodynamically-consistent Monod
40 equation (Jin and Bethke, 2002; 2003),

$$41 r'_R = k \cdot \frac{m_D}{m_D + K_D} \cdot \frac{m_A}{m_A + K_A} \cdot \left[1 - \exp\left(-\frac{\Delta G_A - \Delta G_C}{\chi RT}\right) \right], \quad (1)$$

42 where k is the rate constant (respiration rate per unit biomass, $\text{mol}\cdot\text{g}^{-1}\cdot\text{s}^{-1}$), m_D and m_A are the
43 molal concentrations of electron donors and acceptors, respectively, K_D and K_A are the molal
44 half-saturation constants, ΔG_A is the energy available from redox reactions – the negative of the
45 Gibbs free energy change ($\text{J}\cdot\text{mol}^{-1}$), ΔG_C is the energy conserved by respiration ($\text{J}\cdot\text{mol}^{-1}$), χ is

46 the average stoichiometric number, R is the gas constant ($8.3145 \text{ J}\cdot\text{mol}^{-1}\cdot\text{K}^{-1}$), and T is the
47 temperature in Kelvin. They calculate biosynthesis rate r'_X – biomass production rate per unit
48 biomass (s^{-1}) – from respiration rate,

49
$$r'_X = Y_{X/i} \cdot \nu_{i,R} \cdot r'_R , \quad (2)$$

50 and calculate microbial growth rate ($\text{g}\cdot\text{kg}^{-1}\cdot\text{s}^{-1}$),

51
$$\frac{d[X]}{dt} = (r'_X - r'_M) \cdot [X] , \quad (3)$$

52 as the difference between the biosynthesis rate r'_X and the maintenance/death rate r'_M (s^{-1}) (Jin
53 and Roden, 2011; Jin et al., 2013). Here $[X]$ is the biomass concentration in dry weight per unit
54 water mass ($\text{g}\cdot\text{kg}^{-1}$), $Y_{X/i}$ is the biomass yield per chemical compound i ($\text{g}\cdot\text{mol}^{-1}$), and $\nu_{i,R}$ is the
55 stoichiometric coefficient of compound i in respiration reaction equation. These equations are
56 simple in implementation and fast in computation, but their application to natural environments
57 has not always been successful. For instance, their predictions can deviate from field
58 observations by orders of magnitude (Brown et al., 2000; Chapelle and Lovley, 1990; Murphy
59 and Schramke, 1998). Previous studies have questioned the applicability of the rate equations,
60 and ascribed the discrepancies to the differences in growth conditions and microbial metabolisms
61 between laboratory reactors and natural environments (Jannasch, 1967; Jin and Bethke, 2005; Jin
62 et al., 2013).

63 Recently, genome-scale metabolic models have emerged as a solution to address the
64 challenges of the standard modeling approach (Mahadevan et al., 2011). These models use a
65 series of stoichiometric equations to describe biochemical reactions of metabolic pathways, from
66 nutrient uptake, to respiration, and to biosynthesis (Bordbar et al., 2014; Reed and Palsson,
67 2003). They make possible the integration of metabolic pathways into the prediction of microbial

68 kinetics.

69 For example, dynamic flux balance analysis predicts microbial rates by combining flux
70 balance analysis (FBA) with the Michaelis-Menten equation (fig 1A) (Mahadevan et al., 2002;
71 Vargas et al., 2011). The Michaelis-Menten equation calculates cellular fluxes of nutrient uptake
72 from the environment. FBA is a standard method for analyzing genome-scale metabolic models
73 (Feist and Palsson, 2008; Orth et al., 2010). It takes one or more uptake fluxes as the input, and
74 maximizes growth rates by optimizing the rates of biochemical reactions in genome-scale
75 metabolic models. This method only requires the kinetic parameters for nutrient uptake, and is
76 especially attractive where critical information, such as enzyme kinetic parameters, is not
77 available.

78 Previous studies applied dynamic FBA to both bioreactors and natural environments
79 (Henson and Hanly, 2014; Meadows et al., 2010; Tartakovsky et al., 2013; Zhao et al., 2011;
80 Zhuang et al., 2010). However, the method may not be suitable for many environmental
81 applications. For instance, in order to apply the genome-scale metabolic model of a ferric-iron
82 respirer – *Geobacter sulfurreducens* – to an aquifer, the rate predictions had to be scaled down
83 by an *ad hoc* factor of 10 (Fang et al., 2011; Scheibe et al., 2009).

84 Several factors have been proposed to account for the rate overestimation by dynamic
85 FBA. Specifically, genome-scale metabolic models are under-determined – they have more
86 metabolite fluxes than biochemical reactions (Herrgård et al., 2006). As a result, their solutions
87 might be mathematically correct, but physiologically infeasible. In addition, FBA maximizes
88 microbial growth rates at given nutrient fluxes, which may not work for microbes whose
89 metabolic performance is suboptimal (Feist and Palsson, 2010; Wintermute et al., 2013). Also
90 important is the utilization of the standard Michaelis-Menten equation. This equation does not

91 consider thermodynamic controls on microbial metabolism, and may not capture the full
92 complexity of nutrient transport from the environment to the cytoplasm (Button, 1985; Jin and
93 Bethke, 2007). Furthermore, growth rates and other model predictions are highly sensitive to the
94 enzyme parameters in the Michaelis-Menten equation, which makes dynamic FBA prone to error
95 (Klier, 2012).

96 Here we propose a new method for applying genome-scale metabolic models to microbial
97 kinetics in natural environments (Jin et al., 2013). This method is a hybrid of FBA and the rate
98 laws for microbial respiration and nutrient uptake (Jin and Bethke, 2003). It accounts for
99 microbial energy conservation and the uptake of growth nutrient, and applies FBA independently
100 to the respiration and biosynthesis pathways of genome-scale metabolic models.

101 We illustrate the hybrid method using a representative methanogen –*Methanosarcina*
102 *barkeri*. *M. barkeri* and its relatives live in diverse environments, from surface sediments to
103 aquifers (Hedderich and Whitman, 2006; Smith et al., 2015). They can make methane from
104 acetate – a major contributor to global methane production and a key process of biogeochemical
105 carbon cycling (Ferry, 2010). We apply the hybrid method to simulate the metabolism of *M.*
106 *barkeri* in laboratory reactors, as well as to analyze microbial growth under energy- vs. nutrient-
107 limiting conditions in pristine and biostimulated aquifers.

108 **2. Methods**

109 **2.1. Flux balance analysis**

110 Genome-scale metabolic models represent the biochemical reactions of an entire
111 metabolism using a stoichiometric matrix, \mathbf{S} , of size $m \times n$. Here, n is the number of biochemical
112 reactions and m is the number of metabolites – chemical compounds consumed and produced by
113 biochemical reactions. Element S_{ij} is the stoichiometric coefficient of metabolite i in reaction j .

114 These biochemical reactions are derived from annotated genomes, and drive respiration,
115 biosynthesis, detoxification, and other key metabolic functions (Thiele and Palsson, 2010). In
116 addition, genome-scale metabolic models also contain two hypothetical reactions. One is the
117 biomass production reaction that produces new cells from amino acids, nucleic acids and other
118 biomass precursors, and the other is an ATP hydrolysis reaction that accounts for the energy
119 consumption by cellular maintenance – metabolic processes that maintain the integrity and
120 function of cell components and structures, but do not contribute to cell reproduction (Hoehler
121 and Jørgensen, 2013).

122 FBA assumes that metabolism is at steady state, and applies the principle of mass balance
123 to metabolite fluxes. The result is a linear algebra equation,

$$J = S \cdot R \quad (4)$$

124 where J and R are column vectors; element J_i is the net flux or production rate of metabolite i per
125 unit dry weight of biomass ($\text{mol} \cdot \text{g}^{-1} \cdot \text{s}^{-1}$), and element R_j is the rate of biochemical reaction j per
126 unit biomass ($\text{mol} \cdot \text{g}^{-1} \cdot \text{s}^{-1}$).

127
128 Different modeling disciplines treat under-determined systems differently. For instance,
129 geochemical reaction modeling brings under-determined systems to balance using the principle
130 of mass action (Bethke, 2008). But this approach is not feasible for genome-scale metabolic
131 models because kinetic parameters are not available for most biochemical reactions. Instead,
132 FBA takes one or more uptake fluxes of energy sources and growth nutrients as the input, and
133 optimizes the rates of individual biochemical reactions in order to maximize the rates of growth
134 (Feist and Palsson, 2010).

135 **2.2. Dynamic FBA**

136 Dynamic FBA applies FBA to simulate microbial metabolisms, assuming that the

metabolisms are at quasi steady-state (Becker et al., 2007). At each time step, this method assumes that cell metabolisms are at steady state, and predicts microbial rates and chemical fluxes in two steps (fig 1A) (Mahadevan et al., 2002). It first applies the classical Michaelis-Menten equation to compute the uptake fluxes of energy sources and growth nutrients. For example, the uptake flux F_N of a nutrient is calculated according to,

$$142 \quad F_N = V_{\max} \cdot \frac{m_{N,env}}{m_{N,env} + K_{N,env}}, \quad (5)$$

143 where V_{\max} is the maximum flux ($\text{mol}\cdot\text{g}^{-1}\cdot\text{s}^{-1}$), $m_{\text{N,env}}$ is the molal concentration of nutrient N in
144 the environment, and $K_{\text{N,env}}$ is the molal Michaelis constant (M). It then takes one or more uptake
145 fluxes as the input, and applies FBA to genome-scale metabolic models to predict microbial
146 growth rates and the fluxes of nutrient consumption and waste production by cell metabolisms.
147 At the end of the time step, the growth rates and chemical fluxes are applied to update the
148 concentrations of biomass and chemical compounds, respectively.

149 2.3. Hybrid method

150 We propose a hybrid method that combines FBA with microbial rate laws. This method
151 builds on current frameworks of biogeochemical reaction modeling, and accounts for the
152 availabilities of chemical energy and growth nutrients in the environment (fig 1B).

153 2.3.1. Nutrient uptake

154 A unique feature of the hybrid method is the consideration of cytoplasmic nutrient
155 accumulation. Microbes can accumulate nutrient in the cytoplasm by releasing proton motive
156 force or by hydrolyzing ATP – a process called active transport (Tanford, 1983). By coupling to
157 the release of proton motive force, nutrient transport can be described as

$$158 \quad N_{env} + \nu_H H_{env}^+ \rightleftharpoons N_{cvt} + \nu_H H_{cvt}^+, \quad (6)$$

159 where N_{env} and N_{cyt} are the nutrient in the environment and the cytoplasm, respectively, H_{env}^+ and
 160 H_{cyt}^+ are the protons in the environment and the cytoplasm, respectively, and v_H is the number of
 161 protons transported together with the nutrient. We calculate the uptake flux F_N using the
 162 thermodynamically-consistent Michaelis-Menten equation,

$$163 \quad F_N = V_{\text{max}} \cdot \frac{m_{N,\text{env}}}{m_{N,\text{env}} + K_{N,\text{env}}} \cdot F_T, \quad (7)$$

164 in order to account for the feedback inhibition of nutrient accumulation in the cytoplasm (Jin and
 165 Bethke, 2007). Here F_T is the thermodynamic factor,

$$166 \quad F_T = 1 - \frac{a_{N,\text{env}}}{a_{N,\text{cyt}}} \exp \left[\frac{(z_N + v_H) \cdot F \Delta p}{RT} + z_N \cdot \ln(10) \cdot \Delta \text{pH} \right], \quad (8)$$

167 where a represents chemical activity – the product of molal concentration and activity
 168 coefficient, z_N is the electrical charge of the nutrient, Δp is the proton motive force (V), ΔpH is
 169 the pH difference between the environment and the cytoplasm, and F is the Faraday constant
 170 (Jin, 2012).

171 Evaluating the thermodynamic factor (eq 8) requires knowledge of the nutrient
 172 concentration in the cytoplasm – a parameter not available for most microbes. We note that
 173 cytoplasmic nutrient concentration influences not only nutrient transport (eq 8), but also the
 174 activities of cytoplasmic enzymes that consume nutrients. The impact on nutrient consumption
 175 can be quantified using a kinetic factor F_K ,

$$176 \quad F_K = \frac{m_{N,\text{cyt}}}{m_{N,\text{cyt}} + K_{N,\text{cyt}}}, \quad (9)$$

177 where m and K are the molal concentration and Michaelis constant of nutrients, respectively (Jin
 178 and Bethke, 2007).

179 From equation 8 and 9, we see that high cytoplasmic concentrations inhibit nutrient
180 assimilation by lowering the F_T value and hence the uptake flux F_N . On the other hand, high
181 concentrations raise the kinetic factor F_K and the activities of nutrient-consuming enzymes,
182 thereby promoting nutrient assimilation. We thus assume that to effectively assimilate nutrients,
183 microbes need to maximize the product of the thermodynamic factor F_T and the kinetic factor
184 F_K ,

$$185 \max(F_T \cdot F_K^n). \quad (10)$$

186 Here, the exponent n accounts for the likelihood that the thermodynamic and the kinetic factors
187 may influence nutrient consumption and assimilation to different extents. Solving equation 10
188 gives the optimum cytoplasmic nutrient concentration, which is then applied to compute the
189 nutrient uptake flux (eq 7).

190 2.3.2. Respiration

191 The hybrid method calculates respiration rate r'_R according to the
192 thermodynamically-consistent Monod equation (eq 1). In evaluating this rate equation, we
193 calculate the energy ΔG_C conserved by respiration,

$$194 \Delta G_C = \nu_{ATP} \cdot \Delta G_P, \quad (11)$$

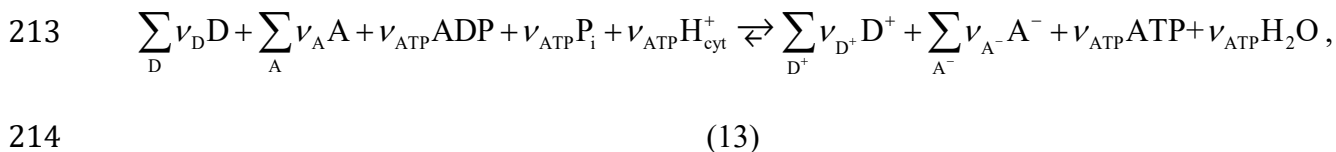
195 as the product of the ATP yield ν_{ATP} – the number of ATPs produced per respiration reaction –
196 and the phosphorylation energy ΔG_P – the energy required for ATP synthesis from ADP and
197 phosphate [$J \cdot (\text{mol ATP})^{-1}$]. We calculate the chemical flux ($\text{mol} \cdot \text{g}^{-1} \cdot \text{s}^{-1}$) of respiration according
198 to

$$199 F_{i,R} = \nu_{i,R} \cdot r'_R, \quad (12)$$

200 where $F_{i,R}$ is the flux of compound i , and its value is positive for reaction products and negative
201 for reactants.

202 We estimate the ATP yield by applying FBA to the respiration pathways in genome-scale
203 metabolic models. ATP is an intermediate metabolite produced by respiration pathways, and is
204 consumed by biosynthesis pathways and maintenance reactions. The steady-state assumption of
205 FBA dictates that the net flux of ATP is 0. In order to estimate ATP yields, we temporarily
206 decouple ATP production and consumption by setting the rates of the biosynthesis and
207 maintenance reactions to 0.

208 We add a hypothetical reaction of ATP output to the genome-scale metabolic models, and
209 assume that respiration maximizes the ATP output flux. We carry out FBA using the uptake
210 fluxes of electron donors D and/or acceptors A as the input. The FBA output includes the fluxes
211 of ATP output and the production of oxidized electron donors D^+ and reduced electron acceptors
212 A^- . The ratios of these fluxes give the stoichiometric equations of respiration,



215 where ν_D and others are stoichiometric coefficients, and P_i is inorganic phosphate (HPO_4^{2-}).

216 2.3.3. Biosynthesis

217 We apply FBA to the biosynthesis pathways to predict the rates, chemical fluxes, and
218 yields of biosynthesis. Biosynthesis pathways use ATP to make new biomass from growth
219 nutrients. As discussed above, because ATP is an intermediate metabolite, we cannot analyze the
220 effect of ATP supply on biosynthesis by applying FBA directly to genome-scale metabolic
221 models. Instead, we stop the ATP-producing respiration pathways and the ATP-consuming
222 maintenance reaction, and prescribe a supply flux of ATP as the input for biosynthesis. In order
223 to analyze the relative importance of ATP and growth nutrients, we also prescribe nutrient
224 uptake fluxes as the input.

225 We follow the standard practice of assuming that microbes maximize the rates of
226 biosynthesis (Feist and Palsson, 2010). The FBA output includes biosynthesis rates r'_x and the
227 chemical fluxes driven by the biosynthetic reactions, such as nutrient consumption and waste
228 production. The ratios of these chemical fluxes can be applied to infer the stoichiometric
229 equation for biosynthesis, and biosynthesis rates are applied to compute the rates of microbial
230 growth (eq 3). The chemical fluxes are combined with those of respiration to compute the total
231 chemical fluxes of cell metabolism. For example, the total flux $F_{i,T}$ of compound i is

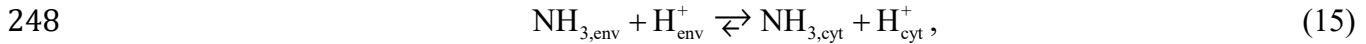
232
$$F_{i,T} = F_{i,R} + F_{i,X}, \quad (14)$$

233 the sum of the fluxes driven by respiration ($F_{i,R}$) and by biosynthesis ($F_{i,X}$).

234 **2.4. Application**

235 We apply the hybrid method to the current genome-scale metabolic model of *M. barkeri*
236 – model iMG746, a revised version of the original model iAF692 (Feist et al., 2006; Gonnerman
237 et al., 2013). We update model iMG746 with the following revisions: the Na^+/H^+ antiporter
238 translocates one proton per Na^+ (Jin, 2012) and the acetate transporter moves one acetate
239 molecule, together with one proton, across the membrane (Welte et al., 2014). We set the
240 growth-associated ATP consumption – the ATP requirement by the hypothetical biomass
241 production reaction – to $109 \text{ mmol} \cdot \text{g}^{-1}$ (Kliphuis et al., 2012). We also follow the original model
242 – iAF692 and remove the sulfite transporter activity, because no gene in *M. barkeri* genome
243 codes for a sulfite transporter.

244 Microbial growth consumes sources of energy, carbon, nitrogen, phosphorous, and other
245 elements. *M. barkeri* can fix N_2 , but prefers ammonium as the source of nitrogen (Kenealy et al.,
246 1982; Kessler et al., 2001), and both pathways are represented in model iMG746. Here we take
247 ammonium uptake as an example (Boogerd et al., 2011),



249 to illustrate how explicitly accounting for nutrient availability and transport influences the
250 accuracy of microbial growth rate prediction via the hybrid method.

251 Before simulating the metabolism of *M. barkeri*, we apply FBA to the methanogenesis
252 pathway of model iMG746 to estimate the yield of ATP (fig 1B). We assume that cytoplasmic
253 ammonium concentrations are at optimum levels for biosynthesis, and solve the optimization
254 problem (eq 10) at different environmental ammonium concentrations using brute-force search.
255 We then use the estimated ATP yield and the optimized cytoplasmic ammonium concentrations
256 to simulate the overall metabolism of *M. barkeri*. At each time step, we first calculate the rate
257 and ATP flux of methanogenesis using the thermodynamically-consistent Monod equation (eqs.
258 1 and 12), and the flux of ammonium uptake using the thermodynamically-consistent Michaelis-
259 Menten equation (eqs. 7 and 8). We predict the rate and chemical fluxes of biosynthesis by
260 applying FBA to the biosynthesis pathway, using the fluxes of ATP synthesis and ammonium
261 uptake as the input. At the end of the time step, we update the concentrations of chemical
262 compounds and biomass in the environment (eqs. 3 and 14). Applying the hybrid method
263 requires a series of microbial and enzymatic parameters, which, for the present calculation, are
264 listed in table 1.

265 We implement the hybrid method by linking the COBRA toolbox and PHREEQC
266 software package and by using the Microsoft Component Object Model (COM) Server as a
267 control and data management source. COM is a Microsoft foundations technology for
268 exchanging information among software packages of different platforms. COBRA and
269 PHREEQC specialize in FBA and biogeochemical reaction modeling, respectively (Charlton and
270 Parkhurst, 2011; Schellenberger et al., 2011). We run COBRA using Gruobi version 6.5, a linear

271 solver that provides acceptable accuracy at small chemical fluxes. The input files of the
272 simulations are available in the Supplementary Material.

273 **3. Results**

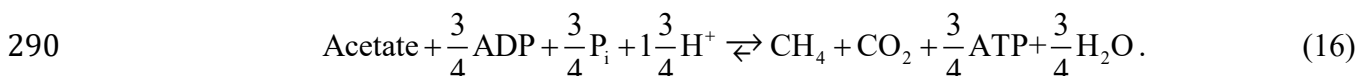
274 We illustrate the hybrid method using the metabolism of *M. barkeri* growing on acetate.
275 We first estimate key parameters, including the ATP yield of methanogenesis, the stoichiometry
276 of biosynthesis reactions, and the flux of ammonium uptake. We then simulate the metabolism in
277 laboratory experiments, and predict the growth in aquifers under energy- vs. nutrient- limiting
278 conditions.

279 **3.1. Model predictions**

280 The hybrid method takes multiple steps to predict the rates of methanogenesis and
281 biosynthesis in *M. barkeri*. These steps include applying FBA independently to the
282 methanogenesis and biosynthesis pathways in model iMG746, as well as the optimization of
283 cytoplasmic nutrient concentration.

284 **3.1.1. ATP yield**

285 We apply FBA to the methanogenesis pathway of model iMG746 to estimate the ATP
286 yield of acetoclastic methanogenesis. The results show that *M. barkeri* makes ATP by
287 consuming acetate and proton and producing methane and CO₂. The ratios of the chemical fluxes
288 give a yield of 0.75 ATPs per methane, and the following stoichiometric equation of
289 acetoclastic methanogenesis,



291 These ratios remain constant over acetate uptake fluxes of 10⁻⁵ mmol·g⁻¹·hr⁻¹, as in oligotrophic
292 environments (Hoehler and Jørgensen, 2013), to a maximum flux of 7.1 mmol·g⁻¹·hr⁻¹ (table 1).
293 The FBA-derived ATP yield matches with the value estimated previously for *Methanosa*

294 species (Welte and Deppenmeier, 2013). The product of the ATP yield and the maximum acetate
295 uptake flux gives the maximum flux of ATP production at $5.3 \text{ mmol}\cdot\text{g}^{-1}\cdot\text{hr}^{-1}$ (eq 12).

296 **3.1.2. Biosynthesis reaction**

297 We apply FBA to the biosynthesis pathway to analyze the effect of microbial energy
298 conservation on biomass synthesis. Biosynthesis consumes both ATP and nutrients. In order to
299 focus on ATP supply, we use the flux of ATP as the only input for FBA, assuming that nutrient
300 uptake is not limiting with respect to biosynthesis, as would be typical in most laboratory
301 experiments (Whitman et al., 2006). Later we consider nutrient limitation by taking ammonium
302 as an example (section 3.3.1.).

303 The FBA results show that the biosynthesis pathway makes new cells by consuming
304 acetate, ammonium, proton, phosphate, and cysteine. The cysteine requirement is consistent with
305 the current practice of laboratory culturing: cysteine is an essential nutrient and serves as a
306 source of sulfur for *M. barkeri* (Mazumder et al., 1986). The biosynthesis pathway also produces
307 CO_2 and methylsulfide (methanethiol or methyl mercaptan, CH_3SH) as waste products. The
308 methylsulfide production complements previous laboratory observations that the methanogenesis
309 of *M. barkeri* can consume methylsulfide as a substrate or produce it as a product (Moran et al.,
310 2008; Zhang et al., 2008).

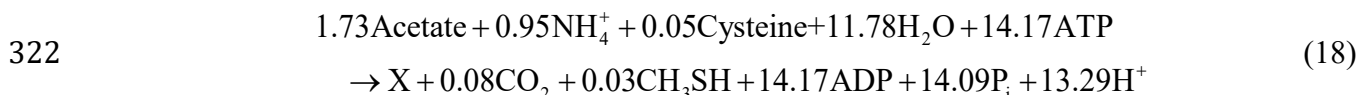
311 The rates and chemical fluxes of biosynthesis vary linearly with ATP fluxes. The overall
312 rate of biosynthesis is given by,

313
$$r'_X = Y_{X/ATP} \cdot F_{ATP}, \quad (17)$$

314 where $Y_{X/ATP}$ is the biomass yield per ATP, and has a value, $6.1 \text{ g}\cdot\text{mol}^{-1}$, that is close to the value
315 ($6.2 \text{ g}\cdot\text{mol}^{-1}$) determined using laboratory bioreactors (Jin, 2012). When ATP is supplied at the
316 maximum production flux, biosynthesis reaches a maximum rate of $3.2 \times 10^{-2} \text{ hr}^{-1}$, consuming

317 ammonium at a maximum flux of $0.35 \text{ mmol}\cdot\text{g}^{-1}\cdot\text{hr}^{-1}$. The predicted maximum biosynthesis rate
318 is close to the maximum growth rate of *M. barkeri* in laboratory reactors ($4.1\times 10^{-2} \text{ hr}^{-1}$)
319 (Fukuzaki et al., 1990).

320 The linear variations of the chemical fluxes also give the following stoichiometric
321 equation for biosynthesis,



323 Here X represents biomass with a chemical formula of $\text{C}_{3.52}\text{H}_{5.42}\text{O}_{1.33}\text{NP}_{0.08}\text{S}_{0.03}$ (molecular
324 weight, 86.46). The chemical formula is arrived at on the basis of the cellular composition of
325 macromolecules and metabolites (Gonnerman et al., 2013); following the common practice, we
326 set the number of nitrogen atom in the biomass formula at 1. The FBA results show that the
327 biosynthesis reaction also produces aminobenzoate and glycolaldehyde as waste products.
328 However, as these compounds have stoichiometric coefficients of only 0.002, they are omitted
329 from the reaction equation. Also note that ADP and phosphate do not have a 1:1 stoichiometry in
330 the products, as would be the case if ATP hydrolysis was the sole reaction involving phosphate.
331 Instead, the smaller quantity of phosphate relative to ADP is due to the consumption of 0.08 mol
332 phosphate per mol biomass synthesized.

333 **3.1.3. Ammonium transport**

334 Optimizing cytoplasmic ammonium concentration requires a series of parameters,
335 including the maximum ammonium uptake flux, the Michaelis constant of cytoplasmic
336 ammonium, and the exponent n (see eqs 8, 9 and 10). We calculate the maximum ammonium
337 uptake flux, V_{\max} , of $0.35 \text{ mmol}\cdot\text{g}^{-1}\cdot\text{hr}^{-1}$, from the maximum biosynthesis rate and the
338 stoichiometric equation of biosynthesis (eq 18). The maximum ammonium flux and biosynthesis

339 rate are close to those of *Geobacter sulfurreducens*: Scheibe et al. (2009) estimated that *G.*
340 *sulfurreducens* has a maximum ammonium flux and biosynthesis rate of $0.5 \text{ mmol} \cdot \text{g}^{-1} \cdot \text{hr}^{-1}$ and
341 $4.7 \times 10^{-2} \text{ hr}^{-1}$, respectively.

342 The exponent n in the optimization function (eq 10) determines the magnitude of
343 ammonium accumulation in the cytoplasm. A large n value favors the accumulation of
344 cytoplasmic ammonium, while a small value lowers the accumulation. Kadam and Boone (1996)
345 analyzed ammonium accumulation by *Methanolobus bombayensis*, *Methanolobus taylorii*, and
346 *Methanohalophilus zhilinaeae* in laboratory reactors where ammonium concentrations are
347 relatively large, $> 10 \text{ mM}$ (fig 2A). By trial and error, we found that by taking the exponent n as
348 2, the optimization solution matches the ammonium accumulation in those three methanogens
349 (see fig 2A). The exponent n of 2 suggests that these methanogens likely favor ammonium
350 accumulation in the cytoplasm, which comes at the expense of decreasing the thermodynamic
351 factor and, hence, the ammonium transport flux (eq 8). This may reflect the need of a relatively
352 large pool of cytoplasmic ammonium in order to speed up the ammonium-consuming enzymes
353 with relatively large Michaelis constants. Specifically, in the cytoplasm of *M. barkeri*,
354 ammonium-consuming enzymes include glutamine synthetase and glutamate dehydrogenase, and
355 their Michaelis constants for ammonium can be as large as 2 mM (Boogerd et al., 2011).

356 Here we assume that for *M. barkeri*, the exponent n also takes a value of 2 and that the
357 laboratory observations can be extrapolated to natural environments, where ammonium
358 concentrations are generally much smaller than 10 mM (fig 2B). Figure 2B and C show the
359 accumulation of cytoplasmic ammonium and the corresponding fluxes of ammonium uptake,
360 given these assumptions. Both the accumulation and uptake respond strongly to the availability
361 of ammonium. With an environmental ammonium concentration of $1 \mu\text{M}$, *M. barkeri* can

362 accumulate ammonium in the cytoplasm by a factor of 33, and transport ammonium at a flux of
363 3.1×10^{-4} mmol·g⁻¹·hr⁻¹. At 10 mM ammonium, the accumulation reduces to four fold, but the
364 uptake flux increases to 0.31 mmol·g⁻¹·hr⁻¹, close to the maximum flux.

365 **3.2. Laboratory experiments**

366 Previous laboratory studies have extensively examined the metabolism of *M. barkeri*
367 growing on acetate (e.g., Mah et al., 1978; Smith and Mah, 1978; Westermann et al., 1989, and
368 others). Here we apply the hybrid method to simulate the experiments of Fukuzaki et al. (1990).
369 They grew *M. barkeri* at 37 °C in batch reactors of 50 mL of complex growth media and 75 mL
370 headspace. The media had pH 7.1 and contained 19.7 mM acetate and 9.3 mM ammonium. They
371 followed closely the progress of acetate consumption, even after acetate reached a constant
372 concentration of 2.0 mM at day 4 (fig 3A), which provides an opportunity to illustrate the
373 thermodynamic control on the progress of metabolism.

374 We simulated the progression of their experiments using an initial biomass concentration
375 of 30 mg·kg⁻¹. This value is estimated on the basis of the experimental results of the first two
376 days (fig 3A). The simulation results match the observations of Fukuzaki et al. (1990). As shown
377 in figure 3A, at the beginning of the experiments, acetate concentration decreases almost linearly
378 with time. After two days into the experiments, the decrease slows down. The simulation
379 predicts that methane and biomass build up in the reactors (fig 3A and B). At the end of the
380 simulation, acetate concentration decreases to 1.3 mM, and 16.9 mmol methane is produced per
381 liter of growth media. Note that our simulation partitions methane between the medium and
382 headspace, with respective volumes as given by Fukuzaki et al. (1990); figure 3 plots only the
383 dissolved methane concentration. These results give a stoichiometric ratio of methane production
384 to acetate consumption at 0.92, close to the value of 1 in the reaction equation (eq 16) (Smith and

385 Mah, 1978). Biomass concentration increases with time and reaches its maximum value at day 5.
386 The simulation also predicts notable ammonium consumption – during the experiments, a total of
387 0.8 mM ammonium is consumed (fig 3A).

388 We also simulate the experimental progress using dynamic FBA, and an initial biomass
389 concentration of 0.12 g·kg⁻¹. Table 1 lists the required parameters and their values for the
390 simulation. As shown in figure 3A and B, dynamic FBA is only applicable to the first 2.5 days of
391 the experiments. It predicts well acetate consumption during this period. But after day 2.5,
392 dynamic FBA fails to return any solution, for reasons described in the discussion below.

393 The results of the hybrid method agree with previous characterizations of methanogen
394 metabolisms. For instance, previous studies describe the efficiency of cell metabolism in terms
395 of the biomass yield per carbon source, $Y_{X/C}$ (Roden and Jin, 2011). We can calculate the
396 biomass yield from the predicted biosynthesis rate r'_X and the total flux of acetate consumption
397 $F_{AC,T}$,

$$398 \quad Y_{X/C} = \frac{r'_X}{F_{AC,T}}. \quad (19)$$

399 Substituting equation 14 and applying the simulation results give a $Y_{X/C}$ value of 4.0 g·mol⁻¹,
400 near the upper end of the range of 1.2 to 4.2 g·mol⁻¹ determined in laboratory bioreactors
401 (Scherer and Sahm, 1981; Sowers et al., 1984).

402 As a second example, acetate is used by *M. barkeri* in both methanogenesis (energy-
403 producing) and biosynthesis (carbon-utilizing) reactions. Here the fractions of acetate consumed
404 by methanogenesis and biosynthesis are denoted as f_R and f_X , respectively. The simulation
405 predicts that *M. barkeri* has f_R of 0.92 and f_X of 0.08 (fig 3C and D), close to the values of 0.95
406 and 0.05 suggested previously (Rittmann and McCarty, 2012).

407 The simulation results include the rates of individual biochemical reactions, which allow
408 us to further track the cellular usage of acetate. The biosynthesis pathway of *M. barkeri*
409 consumes acetate for two purposes. One is the production of acetyl-CoA and pyruvate – the
410 central metabolites for the production of amino acids, nucleotides, and other biomass precursors.
411 The other is the production of reducing power – reduced ferredoxins and cofactor F420, which
412 are utilized in the synthesis of biomass precursors (Jablonski and Ferry, 1991; Krzycki et al.,
413 1982). To produce the reducing power, acetate is first oxidized to methyl-
414 tertahydrosarcinapterin, and then to CO₂. The first oxidation step is driven by the CO
415 dehydrogenase/acetyl-CoA synthase enzyme complex and the second by the reversal of the CO₂
416 reduction portion of the hydrogenotrophic methanogenesis pathway.

417 The simulation results predict that, for *M. barkeri* growing on acetate in laboratory
418 reactors, the biosynthesis pathway spends 72.7% of the acetate flux on the production of acetyl-
419 CoA and pyruvate and the remaining 27.3% on the production of reducing power. Overall, of the
420 total acetate consumed by *M. barkeri*, the fraction used to generate reducing power is 0.02, the
421 fraction used for production of biomass precursors is 0.06, and the remaining fraction, 0.92, is
422 consumed by the methanogenesis pathway for ATP production. These values fall into the range
423 reported previously for *Methanosaeta harundinacea* strain 6Ac – another methanogen capable of
424 acetoclastic methanogenesis. Zhou et al. (2015) analyzed the significance of reducing power
425 production during the growth of strain 6Ac on acetate, and reported that the acetate fraction for
426 reducing power production ranged from 0.005 to 0.037.

427 The simulation results indicate that, in typical laboratory culturing media, the growth of
428 *M. barkeri* is limited primarily by energy sources (Hespell and Bryant, 1979; Tempest and
429 Neijssel, 1984). In the simulation, *M. barkeri* lives in the growth media of about 9 mM

430 ammonium, and can transport ammonium at up to $0.31 \text{ mmol}\cdot\text{g}^{-1}\cdot\text{hr}^{-1}$, fast enough to support the
431 biosynthesis pathway (fig 3D). In comparison, the energy available to ATP synthesis decreases
432 with time, thereby decreasing the flux of ATP production and hence the rate of biosynthesis (fig
433 3C, E, and F).

434 **3.3. Environmental application**

435 Natural environments are often limited in growth nutrients and/or energy sources. But it
436 has been challenging to experimentally analyze how nutrient availability impacts the kinetics of
437 microbial metabolism, due to the technical difficulties in differentiating between metabolically
438 active and dormant cells, in attributing bulk chemical measurements to specific microbial
439 populations, and in untangling the overlapping effects of energy sources and growth nutrients.
440 The hybrid method accounts for ATP production and nutrient consumption at the same time,
441 which offers a computational approach to explore microbial growth under energy- vs nutrient-
442 deprived conditions.

443 **3.3.1. Ammonium limitation**

444 We first take ammonium consumption as an example, and apply the hybrid method to
445 predict how nutrient availability influences the kinetics and efficiency of biomass synthesis of *M.*
446 *barkeri*. Ammonium is commonly limiting in natural environments (Knelman et al., 2014;
447 LeBauer and Treseder, 2008). Its concentrations range from less than 1 μM in oligotrophic
448 environments to over 1 mM in eutrophic settings (Buss et al., 2004). Figure 4A shows how the
449 biosynthesis rate varies with acetate concentration in an environment containing 10 μM
450 ammonium, 1 mM bicarbonate, and 1 to $10^3 \mu\text{M}$ methane. At 1 μM methane, where acetate
451 concentration is less than 30 μM , the biosynthesis is limited by ATP supply, and the biosynthesis
452 rate increases with acetate concentration. At acetate concentration greater than the threshold of

453 30 μM , the biosynthesis is limited by ammonium availability, and proceeds at a maximum rate of
454 $1.9 \times 10^{-4} \text{ hr}^{-1}$.

455 Increases in methane concentration increase the threshold acetate concentration for
456 ammonium limitation. This is because methane accumulation slows down ATP production by
457 methanogenesis (eqs 1 and 12) and therefore reduces the demand for ammonium in biosynthesis
458 (eq 18). At 1 mM methane, the threshold acetate concentration increases to 475 μM , one order of
459 magnitude larger than the acetate threshold at 1 μM methane.

460 Figure 4B illustrates the transition between energy-limited and N-limited regimes across
461 ranges of environmentally-meaningful acetate, ammonium, and methane concentrations.

462 Increases in ammonium concentrations raise maximum biosynthesis rates. Larger ammonium
463 concentrations enable faster ammonium uptake (eq 7), which in turn supports faster biosynthesis
464 (eq 18). At 1 mM ammonium, the biosynthesis can reach a maximum value of $1.2 \times 10^{-2} \text{ hr}^{-1}$,
465 about two orders of magnitude larger than the maximum rate at 10 μM ammonium.

466 The efficiency of biosynthesis has been described using different parameters. As
467 mentioned above, the efficiency of laboratory cultures is characterized using biomass yield $Y_{\text{X/C}}$
468 (eq 19). For natural communities, the efficiency is measured using carbon use efficiency (CUE)
469 – the portion of total carbon consumed in cell metabolism that is assimilated into new biomass
470 (Sinsabaugh et al., 2013; Stefano et al., 2012). The two parameters are exchangeable,

471
$$\text{CUE} = f_{\text{XC}} \cdot \nu_{\text{AC,X}} \cdot Y_{\text{X/C}}, \quad (20)$$

472 where f_{XC} is the fraction of acetate flux assimilated into new biomass over the flux driven by
473 biosynthesis, and $\nu_{\text{AC,X}}$ is the number of acetate molecules consumed per unit biomass
474 synthesized. According to the simulation results, *M. barkeri* has a f_{XC} value of 0.73 and a $\nu_{\text{AC,X}}$
475 value of $0.02 \text{ mol} \cdot \text{g}^{-1}$ (see eq 18).

476 Figure 4C and D show according to the predictions (fig 4A and B), how the biomass
477 yield of *M. barkeri* varies with the concentrations of acetate, ammonium, and methane. Previous
478 studies emphasized the atomic ratios of nutrients, such as Redfield ratio, as a controlling factor
479 of metabolic efficiencies of natural communities (Cleveland and Liptzin, 2007; del Giorgio and
480 Cole, 1998). Figure 4E and F show how the CUE of *M. barkeri* changes with C:N ratios – the
481 atomic ratios of carbon in acetate to nitrogen in ammonium.

482 The predictions suggest that biosynthesis efficiencies depend on the availability of
483 acetate and ammonium. Acetate and ammonium concentrations modulate the fluxes of ATP
484 production and ammonium uptake, respectively (eqs 1 and 7). Where the ATP to ammonium flux
485 ratio is less than or equal to their stoichiometric ratio in the biosynthesis reaction (eq 18), i.e.,
486 20.9, biosynthesis is limited by the supply of ATP. Under this condition, biosynthesis rate varies
487 linearly with ATP production flux (or methanogenesis rate) (eq 17), and the metabolic
488 efficiencies reach their maximum values.

489 Substituting equation 12, 14, and 17 to 19, we can calculate maximum yield (Y_{max}),

$$490 \quad Y_{\max} = \frac{\nu_{\text{ATP}} \cdot Y_{\text{X/ATP}}}{\nu_{\text{AC,R}} + \nu_{\text{ATP}} \cdot \nu_{\text{AC,X}} \cdot Y_{\text{X/ATP}}}, \quad (21)$$

491 from the stoichiometric coefficients of acetate in methanogenesis and biosynthesis ($\nu_{AC,R}$ and
 492 $\nu_{AC,X}$), the ATP yield ν_{ATP} , and the biomass yield per ATP, $Y_{X/ATP}$. Equation 20 and 21 suggest
 493 that maximum metabolic efficiencies are intrinsic microbial parameters constrained by the
 494 properties of metabolic pathways, and their values does not vary with environmental conditions.
 495 For *M. barkeri*, by using the parameter values derived from model iMG746, the maximum yield
 496 Y_{max} is $4.2 \text{ g} \cdot (\text{mol acetate})^{-1}$ and the maximum CUE (CUE_{max}) is 6.1% (figs 4C to F).

497 Where the ratio of ATP to ammonium fluxes surpasses their stoichiometric ratio in the
498 biosynthesis reaction (eq 18), the biosynthesis rate no longer responds to the changes in acetate

499 concentration or methanogenesis rate but, instead, is determined solely by the uptake flux of
500 ammonium,

501
$$r'_X = Y_{X/N} \cdot F_N , \quad (22)$$

502 where $Y_{X/N}$ is the biomass yield per ammonium. The predictions (fig 4B) give a $Y_{X/N}$ value of
503 $91.5 \text{ g} \cdot (\text{mol } \text{NH}_4^+)^{-1}$ for *M. barkeri*, which is close to the value of $121 \text{ g} \cdot (\text{mol } \text{NH}_4^+)^{-1}$
504 determined in laboratory for *Methanothermobacter thermautotrophicus* (Kenealy et al., 1982).
505 The decoupling of biosynthesis from methanogenesis has been observed for *M. barkeri* growing
506 under ammonium-deprived conditions (Kenealy et al., 1982).

507 Under the conditions of ammonium limitation, metabolic efficiencies are not constant,
508 but decrease nonlinearly with increasing acetate concentrations or increasing C:N ratios (figs 4C
509 to F). These predictions agree with the CUE values reported for natural communities. In natural
510 environments, ammonium concentrations tend to be small and thus likely limit the biosynthesis
511 of natural communities. Accordingly, the CUE declines nonlinearly with C:N ratios (del Giorgio
512 and Cole, 1998).

513 Where acetate concentrations are much larger than the half-saturation constant of acetate
514 consumption (i.e., 5 mM for *M. barkeri*, table 1), the efficiencies reach their minimum values
515 (figs 4C to F). Minimum efficiencies can be calculated from equation 19 and 22 by assuming
516 that methanogenesis proceeds at its maximum rate. For example,

517
$$Y_{\min} = \frac{Y_{X/N} \cdot F_N}{\nu_{AC,R} \cdot k + \nu_{AC,X} \cdot Y_{X/N} \cdot F_N} . \quad (23)$$

518 According to this equation, the minimum efficiencies depend not only on the properties of
519 metabolic networks but also on the uptake flux or the availability of ammonium. In natural
520 environments with ammonium concentrations less than 10 μM , the minimum biomass yields and

521 CUEs can be as low as $0.027 \text{ g} \cdot (\text{mol acetate})^{-1}$ and 0.04%, respectively – two orders of
522 magnitude smaller than the predicted maximum efficiencies (Y_{\max} and CUE_{\max}). On the other
523 hand, in laboratory reactors, where ammonium is supplied at concentrations greater than 1 mM
524 (Whitman et al., 2006), the minimum yields are greater than $1.45 \text{ g} \cdot (\text{mol acetate})^{-1}$, close to the
525 predicted Y_{\max} value. In other words, the biomass yields determined in laboratory bioreactor
526 should be close to each other, but the CUEs of natural communities can vary over orders of
527 magnitude. These predictions are consistent with the results of previous laboratory and field
528 studies: the biomass yields of *M. barkeri* in laboratory reactors fall into a relatively narrow range
529 of 1.2 to $4.2 \text{ g} \cdot (\text{mol acetate})^{-1}$ (Scherer and Sahm, 1981; Sowers et al., 1984), and the CUEs of
530 natural communities vary more than an order of magnitude (del Giorgio and Cole, 1998).

531 Combining equation 12, 17, and 22, biosynthesis rates r'_x can be calculated according to

532
$$r'_x = \min(Y_{X/ATP} \cdot v_{ATP} \cdot r'_R, Y_{X/N} \cdot F_N). \quad (24)$$

533 This equation states that biosynthesis is subject to Liebig's Law of the Minimum (Bader, 1978;
534 Droop, 1974; Egli, 2013; Zinn et al., 2004), and biosynthesis rate is determined either by ATP
535 production flux F_{ATP} or by ammonium uptake flux F_N , depending on which one places a stronger
536 limitation and whether or not biosynthesis is coupled to methanogenesis.

537 **3.3.2. Growth kinetics**

538 According to the above biosynthesis predictions (fig 4B), ammonium availability in the
539 environment can place upper limits on the rates of biosynthesis (Kessler et al., 2001; LeBauer
540 and Treseder, 2008; Ma and Thauer, 1990). These limits may account for the wide range of
541 doubling time reported for microbes. For example, where the energy sources and growth
542 nutrients are abundant, the hybrid method predicts that *M. barkeri* has a maximum biosynthesis
543 rate of $3.2 \times 10^{-2} \text{ hr}^{-1}$, which is equivalent to a doubling time of 22 hours. This prediction is close

544 to the doubling time of 24 hours determined for *M. barkeri* in laboratory bioreactors (Peinemann
545 et al., 1988; Smith and Mah, 1978).

546 The doubling time of natural microbes is much longer than laboratory cultures. Phelps et
547 al. (1994a) estimated that, in the sediments of Lake Mendota, a eutrophic lake in Wisconsin,
548 USA, microbes have a doubling time of 5 to 10 days. At the observed sediment ammonium
549 concentration of approx. 100 μM (Austin and Lee, 1973), the hybrid method predicts a N-limited
550 growth rate for *M. barkeri* of $2.2 \times 10^{-3} \text{ hr}^{-1}$ (doubling time of 13 days), close to the estimate of
551 Phelps et al. (1994a).

552 In the Middendorf aquifer, South Carolina, USA, microbes have an average doubling
553 time of centuries (Phelps et al., 1994a). In this aquifer, the groundwater has about 1 μM
554 ammonium (Phelps et al., 1994b). According to the above predictions, *M. barkeri* growing at 1
555 μM ammonium has a biosynthesis rate up to $2 \times 10^{-5} \text{ hr}^{-1}$, a value that is close to microbial
556 maintenance rate. In natural environments of limited resources, microbes may have maintenance
557 rates an order of magnitude smaller than laboratory cultures (Schmidt, 1992). Using a
558 maintenance rate of $1.8 \times 10^{-5} \text{ hr}^{-1}$ (table 1), *M. barkeri* would have a growth rate of $2 \times 10^{-6} \text{ hr}^{-1}$
559 (eq 3), equivalent to a doubling time of 40 years. Other factors, such as non-optimal temperatures
560 and pHs and the scarcity of energy sources and other growth nutrients, can also slow down
561 growth, further extending the doubling time of aquifer microbes (Price and Sowers, 2004).

562 **3.3.3. Pristine aquifer**

563 The potential linkage between the long doubling time of aquifer microbes and the low
564 ammonium in groundwater suggests that the growth of aquifer microbes might be limited by the
565 availability of ammonium. Current biogeochemical reaction modeling calculates biosynthesis
566 rates as a linear function of methanogenesis rates (eq 2), assuming that the growth of natural

567 microbes is limited primarily by energy sources (Jin et al., 2013). Here we use *M. barkeri* as a
568 model microbe and test in pristine aquifers, whether the ammonium limitation on growth is
569 applicable to aquifer microbes.

570 We retrieved groundwater chemistry data from the U.S. Geological Survey (USGS)
571 National Water Information System (NWIS) database (<https://nwis.waterdata.usgs.gov>). We
572 searched the database for samples that were collected from wells (site type) and analyzed for
573 ammonium (USGS parameter 00608), methane (parameter 76994), and dissolved oxygen
574 (parameter 00300). We eliminated samples that contained 1 mg/L or more dissolved oxygen, as
575 likely being inhibitory for methanogenesis. Out of the 21 hydrologic regions in the database, the
576 Mid-Atlantic region returned the largest number (i.e., 170) of groundwater samples (see
577 Supplementary Material). These samples were from the siliciclastic aquifers in Pennsylvania,
578 USA – the aquifers of unconsolidated sediments, sandstones, siltstones, and shale (Ator et al.,
579 2005). They have an average temperature of 12 °C, pH of 7.8, about 0.3 mM bicarbonate, and 4
580 µM methane. No acetate analysis is available for these samples. But in pristine aquifers, acetate
581 can reach a concentration of 20 µM (McMahon and Chapelle, 1991a; 1991b).

582 The hybrid method predicts that *M. barkeri* in the aquifers has a biosynthesis rate of
583 $6.8 \times 10^{-5} \text{ hr}^{-1}$. Taking the maintenance rate as $1.8 \times 10^{-5} \text{ hr}^{-1}$ (table 1), *M. barkeri* would have a
584 growth rate of $5.0 \times 10^{-5} \text{ hr}^{-1}$ (eq 3) or a doubling time of 578 days. If we neglected ammonium
585 limitation and calculated the biosynthesis rate using the linear biosynthesis equation (eq 2), we
586 would arrive at a growth rate of $8.5 \times 10^{-5} \text{ hr}^{-1}$ or 339 days. Considering that we assume a
587 relatively large acetate concentration (i.e., 20 µM), the difference between the two predictions
588 might indicate that at least at some locations of the aquifers, microbial growth is limited by
589 ammonium availability.

590 The potential ammonium limitation is consistent with the groundwater chemistry of the
591 aquifers. Figure 5 compares the concentrations of methane and ammonium in the groundwater.
592 Methane levels range from below 1 μM to over 100 μM , and correlate moderately with the
593 concentrations of ammonium (Spearman's coefficient, 0.495). If the ammonium availability
594 limits methanogen growth in the aquifers, it would also limit the production of methane gas.

595 **3.3.4. Bioremediation**

596 As a second example, we take *M. barkeri* as a model methanogen, and apply the hybrid
597 method to predict the growth of aquifer methanogens during *in situ* groundwater bioremediation.
598 Current *in situ* bioremediation practice removes or immobilizes groundwater contaminants by
599 injecting solutions of organic compounds into aquifers and by stimulating the metabolisms of
600 aquifer microbes (Majone et al., 2015).

601 We focus on a field bioremediation experiment in an alluvial aquifer, Colorado, USA
602 reported by Mouser et al. (2009). This experiment injected acetate solution into the aquifer
603 through a 10-meter-long array of injection wells, and monitored the chemistry and microbiology
604 in the groundwater from monitoring wells 2.5 meters (well D-02 and 04) to 5 meters (well D-05
605 and 08) down-gradient from the injection wells. The acetate injection stimulated the metabolisms
606 of aquifer microbes, including methanogens (Anderson et al., 2003; Komlos et al., 2008; Liang
607 et al., 2012). We assume that the biostimulation increased microbial metabolic rates, including
608 maintenance rates (van Bodegom, 2007). As a result, in the biostimulated aquifer, *M. barkeri*
609 may have a maintenance rate close to the value of $1.8 \times 10^{-4} \text{ hr}^{-1}$ determined in laboratory
610 bioreactors (Wandrey and Aivasidis, 1983).

611 Figures 6A to D show, during the experiment, how the ATP flux from acetoclastic
612 methanogenesis varied with time (eqs 1 and 12). The ATP fluxes are predicted from the reported

613 acetate concentrations during the experiment (Mouser et al., 2009, their figure 1B), and by taking
614 pH of the groundwater at 7, bicarbonate at 3.4 mM, and methane at 0.1 μ M (Druhan et al., 2014;
615 Fang et al., 2009).

616 The variations in ATP fluxes reflected the acetate concentrations in the groundwater. The
617 acetate injection occurred during the first 10 days and between day 17 and 30 of the experiment
618 (Mouser et al., 2009). Accordingly, the ATP fluxes increased and then decreased during the first
619 20 days. Afterwards, the fluxes increased again. Also, the maximum ATP fluxes were larger in
620 the wells close to the injection wells (well D-02 and 04) than in those away from the injection
621 (well D-05 and 08).

622 Figure 6E to H show how the ammonium uptake fluxes varied with time. The ammonium
623 fluxes reflected the ammonium concentrations in the groundwater, which were different at
624 different locations. These differences have been attributed to the heterogeneous occurrence of
625 sedimentary organic matter (Mouser et al., 2009).

626 Figure 6I to L show the predicted growth rates of *M. barkeri*. In well D-02, 04, and 05,
627 the variations follow the trends of ammonium fluxes. In well D-02, the growth rate of *M. barkeri*
628 increases with time to 2.3×10^{-3} hr⁻¹. In well D-04, the growth rate remains relatively constant at
629 $1.1 \pm 0.3 \times 10^{-3}$ hr⁻¹. In well D-05, the growth rate remains close to 0. In contrast, in well D-08, the
630 variation in growth rate is similar to that of ATP production flux. These results suggest that in
631 well D-02, 04, and 05, the biosynthesis of *M. barkeri* is limited by ammonium availability and
632 hence is decoupled from methanogenesis. On the other hand, in well D-08, the biosynthesis is
633 limited by ATP production (or by acetate availability) and is coupled to methanogenesis.

634 The metabolic decoupling is also evident from the predicted CUEs (figs 6M to P). In well
635 D-02, 04, and 05, at most sampling time points, the CUEs remain smaller than the maximum

636 value of 6.1%, reaching as low as 0.06% in well D-05. However, in well D-08, the CUEs remain
637 constant at the maximum value throughout the experiments.

638 The growth rate predictions suggest that methanogens would not be able to flourish
639 around well D-05, but they could live and develop around well D-02, 04, and 08. In the aquifer,
640 the main source of ammonium was from the degradation of sedimentary organic matter (Mouser
641 et al., 2009). This natural nitrogen source was insufficient to support the metabolisms of aquifer
642 microbes during the biostimulation (fig 6I to P). Thus the addition of acetate, without any source
643 of nitrogen, might have hindered the stimulation of aquifer microbes. In addition, the
644 heterogeneous distribution of ammonium can account, at least in part, for the uneven spatial
645 distribution of microbes in the aquifer and their metabolic activities during biostimulation tests
646 (Liang et al., 2012).

647 If we neglected the impact of ammonium and assumed a linear relationship between
648 biosynthesis and methanogenesis (eq2), as in current practice of biogeochemical reaction
649 modeling (Li et al., 2009; Yabusaki et al., 2011), we would arrive at growth rates up to an order
650 of magnitude larger than the values predicted by the hybrid method (see figs 7I to L). These
651 differences reflect the limiting effect of ammonium in aquifers, and resonate with the previous
652 notion that current modeling frameworks (eqs 1 to 3) may not capture accurately the rates of
653 microbial metabolisms *in situ* (Brown et al., 2000; Murphy and Schramke, 1998; Phelps et al.,
654 1994a).

655 We can test the occurrence of ammonium limitation on the basis of gene expression.
656 Specifically, *M. barkeri* and other prokaryotes accumulate ammonium in the cytoplasm using
657 ammonium transporter enzyme. Mouser et al. (2009) analyzed the expression of the enzyme by
658 the aquifer microbes during the field experiment. They enumerated the transcripts of an

659 ammonium transporter gene, *amtB*, using reverse-transcription polymerase chain reaction (RT-
660 PCR), and compared the transcript numbers to those of a housekeeping gene *recA* (fig 7). A
661 BLAST search against currently available genome sequences found that their primer sets for
662 *amtB* retrieved sequences from diverse microbes, including *M. barkeri*. Their results thus might
663 have reflected the response of aquifer microbes in general.

664 We quantify the significance of ammonium limitation using the ratio of ammonium
665 concentration m_{env} in groundwater to the concentration m_{req} required to support the
666 stoichiometrically-balanced biosynthesis of *M. barkeri*. Figures 6Q to T compare the ammonium
667 concentration in the groundwater to the concentrations required by the stoichiometrically-
668 balanced growth. Figure 7 shows that during the field experiments, the expression of *amtB* gene
669 correlated with the significance of ammonium limitation (Spearman's coefficient of -0.852). The
670 strong negative correlation is consistent with our assessment about the ammonium limitation
671 around well D-02, 04, and 05.

672 **4. Discussion**

673 We illustrated in this paper how to predict the kinetics of microbial metabolisms by
674 combining genome-scale metabolic models with thermodynamically-consistent rate laws. We
675 took methanogenesis as an example and simulated the metabolism of *M. barkeri* in both
676 laboratory bioreactors and aquifers. The results show that the new method expands and improves
677 the predictions of microbial kinetics, and can be applied to diverse environments, from
678 laboratory bioreactors of optimal growth conditions to natural environments of limited resources.

679 **4.1. Method development**

680 The hybrid method follows dynamic FBA, and uses genome-scale metabolic models to
681 account for the pathways of cell metabolisms (fig 1). But the two methods differ from each other

682 in the treatment of metabolic pathways (fig 1). Dynamic FBA uses standard genome-scale
683 metabolic models, which lump together the biochemical reactions of catabolic and biosynthetic
684 pathways. Additionally, they use a hypothetical ATP-consuming reaction to account for the
685 energy demand by maintenance (Thiele and Palsson, 2010). For this reason, direct applications
686 of genome-scale metabolic models require that ATP production fluxes from catabolism surpass
687 ATP hydrolysis rates of maintenance. As a consequence, dynamic FBA always predicts that
688 microbes are actively growing. But in most subsurface environments, active growth might be
689 sporadic because of limited energy sources and growth nutrients, and stationary and death phases
690 can be the common metabolic states (Morita, 1997; Price and Sowers, 2004; Roszak and
691 Colwell, 1987).

692 In comparison, the hybrid method applies FBA separately to the catabolic and
693 biosynthetic pathways in genome-scale metabolic models and, following standard practice in
694 biogeochemical modeling, accounts for cellular maintenance using negative rates of biosynthesis
695 (Jin and Roden, 2011; Jin et al., 2013). The separate treatment of catabolic, biosynthetic, and
696 maintenance pathways enables the application of the hybrid approach to a wider range of
697 metabolic states, from active growth to stationary and to death phase. For example, in the
698 simulation of the laboratory experiments, dynamic FBA fails to find a solution after 2.5 days into
699 the experiments. After this point, the ATP flux from methanogenesis is no longer able to match
700 the ATP consumption flux by maintenance assumed in model iMG746 (fig 3A, B, and E). On the
701 other hand, the hybrid method predicts that the metabolism of *M. barkeri* follows the typical
702 sequence of exponential and stationary phases (fig 3B).

703 The hybrid method predicts microbial kinetics by combining genome-scale metabolic
704 models with rate laws. There are different microbial rate laws on which to potentially build this

705 application (Simkins and Alexander, 1984). The choice of the thermodynamically-consistent
706 Monod equation (eq 1) reflects the need to consider thermodynamics in predicting the kinetics of
707 microbes under the conditions that frequently characterize natural systems (Jin and Bethke,
708 2005). As demonstrated in the example application (figs 3C, D, and F), the hybrid method
709 captured the response of acetate consumption flux to the changes in the chemical energy of the
710 environment: the acetate fluxes are larger at larger available energies, and vice versa. If we
711 applied dynamic FBA without accounting for the thermodynamics of microbial catabolism, we
712 would not be able to capture the response of acetate fluxes to the thermodynamic conditions of
713 the environment (fig 3A and F).

714 Applying the hybrid method requires the evaluation of the thermodynamically-consistent
715 rate laws and the simulation of biosynthesis using FBA. In the example application to laboratory
716 experiments (fig 3), we coupled FBA directly to the evaluation of the rate laws. At each iteration,
717 we use the rate laws to compute the fluxes of ATP synthesis and nutrient uptake, and feed the
718 fluxes to FBA to obtain biosynthesis rates (fig 1B). The direct coupling ensures a rigorous and
719 real-time exchange of microbial rates and fluxes between the rate laws and FBA, but running
720 FBA at every iteration can be computationally expensive – especially in field-scale applications
721 that repeat FBA at every grid cell and time step.

722 Alternatively, we can couple FBA and microbial rate laws indirectly by replacing FBA in
723 the hybrid method with Liebig's Law of the Minimum (eq 24). According to the FBA
724 predictions, biosynthesis rates are determined by the most limiting fluxes of ATP production and
725 nutrient uptake, and the relationship can be described according to Liebig's Law of the
726 Minimum. Thus rather than running the time-consuming FBA at each iteration, we can arrive at
727 the same results by the simple evaluation of Liebig's Law of the Minimum. Specifically, we first

728 apply FBA to biosynthesis pathways to estimate the biomass yields for ATP and for relevant
729 growth nutrients and to build Liebig's Law of the Minimum for biosynthesis (eq 24). We then
730 compute metabolic rates by combining the thermodynamically consistent rate laws for
731 respiration and nutrient uptake and Liebig's Law of the Minimum for growth.

732 **4.2. Methanogenesis**

733 Methanogenesis is a final step of organic matter degradation, and methane fluxes are a
734 key parameter in predicting future environmental changes (Nisbet et al., 2016; Thauer et al.,
735 2008). Previous studies predicted the metabolic activities of methanogens using dynamic FBA
736 (Stolyar et al., 2007) and microbial rate laws (Jin and Roden, 2011; Yang and Okos, 1987). Here
737 we applied the hybrid method and predicted the metabolic rates and chemical fluxes of *M.*
738 *barkeri* in both laboratory reactors and aquifers.

739 The hybrid method enhances the predictions of microbial carbon fluxes by accounting for
740 biochemical mechanisms at the enzyme level. By applying FBA to genome-scale metabolic
741 models, the hybrid method tracks not only the total fluxes of carbon, but also the contribution of
742 different biochemical pathways. In the application to the laboratory experiments (fig 3), in
743 addition to acetoclastic methanogenesis, the growth of *M. barkeri* also consumes acetate using
744 two different pathways – the reversal of CO₂ reduction pathway that generates reducing power
745 by oxidizing acetate to CO₂ and the biosynthesis pathway that assimilates acetate into new
746 biomass. Specifically, the pathways of methanogenesis, acetate assimilation, and reducing power
747 production consume 92%, 6%, and 2% of the total acetate fluxes, respectively. These fractions
748 reflect how *M. barkeri* allocates acetate to the three pathways in order to meet its needs of ATP,
749 carbon, and reducing power for biosynthesis.

750 The hybrid method is organism-specific – its predictions are based on genome-scale

751 metabolic models of individual organisms and their kinetic parameters of respiration,
752 maintenance, and nutrient uptake. But *M. barkeri* and other methanogens rarely live alone in
753 natural environments. Instead, they mingle with each other, and partner with diverse fermenting
754 microbes, sulfate reducers, acetogens, and others of different metabolic functions to build
755 microbial communities and to carry out organic matter degradation, nutrient cycling, and other
756 ecological functions (Nielsen et al., 2011; Schimel and Schaeffer, 2012).

757 Applying the hybrid method to microbial communities is feasible, provided that genome-
758 scale metabolic models of key community members are available. The application assumes that
759 the metabolisms of community members are at quasi steady state, and applies iterative
760 procedures to track the progress of community metabolisms (Zhuang et al., 2010). At each time
761 step of simulation, the hybrid method is applied to individual community members, and the
762 results are combined to compute the total fluxes of microbial communities, and to update the
763 abundances of community members and the concentrations of chemical compounds in the
764 environment. Such applications may hold promise for probing the ecological functions of
765 microbial communities and their dependence on environmental conditions – for example, the
766 contribution of different methanogens to methane fluxes and how environmental conditions
767 dictate the development and function of microbial communities (Keller and Bridgham, 2007; Ye
768 et al., 2012).

769 **4.3. Microbial growth**

770 The hybrid method can be applied to microbial metabolism under energy- vs. nutrient-
771 limiting conditions. We illustrated this capability by analyzing the growth of *M. barkeri* across
772 wide spectra of acetate and ammonium availabilities (fig 4). The results confirm that linear
773 growth equations (e.g., eqs 2 and 3) are best applied to laboratory bioreactors and eutrophic

774 environments, where nutrients are abundant. Under this condition, biosynthesis is limited by
775 ATP synthesis, and is coupled to respiration (Russell and Cook, 1995; Tempest and Neijssel,
776 1984). The results also show that in natural environments, biosynthesis rates are determined by
777 the fluxes of either ATP production or ammonium uptake, depending on which one places a
778 stronger limitation (eq 24).

779 The hybrid method is universal, and can also be applied to other growth nutrients by
780 explicitly accounting for the uptake and consumption of the nutrients. For example, if we expand
781 the application and consider the availability of phosphate – another limiting nutrient for natural
782 microbes (Elser et al., 2007), we would arrive at similar results. Specifically, biosynthesis rates
783 are subject to Liebig’s Law of the Minimum, and are determined by the factors of most
784 significant limitation,

785
$$r'_X = \min(Y_{X/ATP} \cdot v_{ATP} \cdot r'_R, Y_{X/N} \cdot F_N, Y_{X/P} \cdot F_P), \quad (25)$$

786 where $Y_{X/P}$ is the biomass yield per phosphate, and F_P is the flux of phosphate uptake. The $Y_{X/P}$
787 value can be determined from the variations in biosynthesis rate with phosphate uptake flux, and
788 the value is $1.1 \times 10^3 \text{ g} \cdot (\text{mol phosphate})^{-1}$. Similar to the above predictions of ammonium
789 limitation, where phosphorus is limiting, biosynthesis is also decoupled from methanogenesis – a
790 prediction consistent with laboratory observations (Archer, 1985).

791 The agreement between the hybrid method and Liebig’s Law of the Minimum arises from
792 the similar underlying assumptions of the two methods. Liebig’s Law of the Minimum assumes
793 that the pathways of respiration and nutrient utilization do not interact with each other, and
794 biosynthesis rates are determined by the more limiting of ATP supply or nutrient uptake fluxes
795 (Zinn et al., 2004). The hybrid method takes the fluxes as inputs. These fluxes are independent of
796 each other and meet the energy and element needs of biosynthesis pathways. As a result, the

797 most limiting flux determines the rate of biosynthesis (Edwards et al., 1999; Orth et al., 2010).
798 In addition to the linear growth equation (eqs 2 and 3) and Liebig's Law of the Minimum
799 (eqs 3 and 25), other equations have also been applied to predict microbial growth. For instance,
800 previous studies accounted for growth nutrient limitation using the multiplicative Monod
801 equation (Bader, 1982; Jin et al., 2013; MeGee et al., 1972). This model quantifies the effect of
802 nutrient availability using a Monod-type factor, and computes biosynthesis rates according to

$$803 \quad r'_X = Y_{X/i} \cdot v_{i,R} \cdot r'_R \cdot \frac{m_{N,env}}{m_{N,env} + K_{N,env}}. \quad (26)$$

804 This model assumes that the pathways of respiration interact with those of growth nutrient
805 consumption, and should be accounted for at the same time (Zinn et al., 2004).

806 Previous studies also predicted microbial growth using sigmoidal functions, such as the
807 logistic equation and the Gompertz equation (Zwietering et al., 1990). These functions focus on
808 biomass concentrations, and assume *a priori* that microbial growth follows a sigmoid function.
809 They calculate biomass concentrations from lag time, maximum growth rate, and maximum
810 biomass concentration of the environment, and hence offer limited link to respiration pathways
811 (Mitchell et al., 2004). For this reason, they may not be the best option for biogeochemical
812 reaction modeling – a modeling discipline that emphasizes the chemical interactions between
813 microbial metabolisms and natural environments.

814 In summary, we proposed a hybrid method that combines FBA with rate laws to predict
815 the kinetics of microbial metabolism in natural environments. This method accounts for the
816 availability of energy sources and growth nutrients, and applies FBA independently to the
817 respiration and the biosynthesis pathways of genome-scale metabolic models. The application to
818 *M. barkeri* in laboratory experiments shows that the method explicitly tracks cellular fluxes of
819 energy and carbon, thereby bringing unprecedented metabolic detail to biogeochemical reaction

820 modeling. The applications to aquifers show that the growth of natural methanogens is limited
821 either by energy sources or by the most limiting nutrient, and can be described according to
822 Liebig's Law of the Minimum. These predictions are consistent with the decoupling of
823 biosynthesis from methanogenesis and the slow growth of natural microbes under
824 nutrient-deprived conditions, the correlation between dissolved methane and ammonium in the
825 pristine aquifers of Pennsylvania, USA, and the expression of ammonium transporter gene in the
826 biostimulated alluvial aquifer of Colorado, USA.

827 **Acknowledgement:** This research was funded by National Aeronautics and Space
828 Administration under Grant NNX16AJ59G and by the National Science Foundation under
829 Award EAR-1636815. We thank the four reviewers for their constructive comments. Q.J. also
830 thanks the hospitality of the Isaac Newton Institute for Mathematical Sciences, University of
831 Cambridge, UK, where the work was initiated.

832 **Supplementary Information**

833 1. Mendeley Data: A MATLAB code for simulating the metabolism of *Methanosarcina*
834 *barkeri* by linking COBRA toolbox with PHREEQC.
835 2. Groundwater chemistry data from the Mid Atlantic hydrologic region.

836

837 **References**

838 Anderson, R.T., Vrionis, H.A., Ortiz-Bernad, I., Resch, C.T., Long, P.E., Dayvault, R., Karp, K.,
839 Marutzky, S., Metzler, D.R., Peacock, A., White, D.C., Lowe, M. and Lovley, D.R.
840 (2003) Stimulating the *in situ* activity of *Geobacter* species to remove uranium from the
841 groundwater of a uranium-contaminated aquifer. *Applied and Environmental*
842 *Microbiology* 69, 5884-5891.

843 Archer, D.B. (1985) Uncoupling of Methanogenesis from Growth of *Methanosarcina barkeri* by
844 Phosphate Limitation. *Applied and Environmental Microbiology* 50, 1233-1237.

845 Ator, S.W., Denver, J.M., Krantz, D.E., Newell, W.L. and Martucci, S.K. (2005) A surficial
846 hydrogeologic framework for the Mid-Atlantic Coastal Plain. US Geological Survey.

847 Austin, E.R. and Lee, G.F. (1973) Nitrogen Release from Lake Sediments. *Journal (Water*
848 *Pollution Control Federation*) 45, 870-879.

849 Bader, F.B. (1982) Kinetics of double-substrate limited growth, in: Bazin, M.J. (Ed.), *Microbial*
850 *Population Dynamics*. CRC Press, Inc., Boca Raton, FL, pp. 1-32.

851 Bader, F.G. (1978) Analysis of double-substrate limited growth. *Biotechnology and*
852 *Bioengineering* 20, 183-202.

853 Becker, S.A., Feist, A.M., Mo, M.L., Hannum, G., Palsson, B.Ø. and Herrgard, M.J. (2007)
854 Quantitative prediction of cellular metabolism with constraint-based models: the COBRA
855 Toolbox. *Nature Protocols* 2, 727-738.

856 Bethke, C.M. (2008) *Geochemical and Biogeochemical Reaction Modeling*, 2nd ed. Cambridge
857 University Press, Cambridge, UK.

858 Boogerd, F.C., Ma, H., Bruggeman, F.J., van Heeswijk, W.C., García-Contreras, R., Molenaar,
859 D., Krab, K. and Westerhoff, H.V. (2011) AmtB-mediated NH₃ transport in prokaryotes
860 must be active and as a consequence regulation of transport by GlnK is mandatory to
861 limit futile cycling of NH₄⁺ / NH₃. *FEBS Letters* 585, 23-28.

862 Bordbar, A., Monk, J.M., King, Z.A. and Palsson, B.O. (2014) Constraint-based models predict
863 metabolic and associated cellular functions. *Nature Reviews Genetics* 15, 107-120.

864 Brown, C.J., Schoonen, M.A.A. and Candela, J.L. (2000) Geochemical modeling of iron, sulfur,
865 oxygen and carbon in a coastal plain aquifer. *Journal of Hydrology* 237, 147-168.

866 Buss, S.R., Herbert, A.W., Morgan, P., Thornton, S.F. and Smith, J.W.N. (2004) A review of
867 ammonium attenuation in soil and groundwater. *Quarterly Journal of Engineering*

868 Geology and Hydrogeology 37, 347-359.

869 Button, D.K. (1985) Kinetics of nutrient-limited transport and microbial growth. *Microbiol. Mol.*
870 *Biol. Rev.* 49, 270-297.

871 Button, D.K. (1998) Nutrient uptake by microorganisms according to kinetic parameters from
872 theory as related to cytoarchitecture. *Microbiology and Molecular Biology Reviews* 62,
873 636-645.

874 Chang, A., Schomburg, I., Placzek, S., Jeske, L., Ulbrich, M., Xiao, M., Sensen, C.W. and
875 Schomburg, D. (2014) BRENDA in 2015: exciting developments in its 25th year of
876 existence. *Nucleic Acids Research*.

877 Chapelle, F.H. and Lovley, D.R. (1990) Rates of microbial metabolism in deep coastal plain
878 aquifers. *Applied and Environmental Microbiology* 56, 1865-1874.

879 Charlton, S.R. and Parkhurst, D.L. (2011) Modules based on the geochemical model PHREEQC
880 for use in scripting and programming languages. *Computers & Geosciences* 37, 1653-
881 1663.

882 Cleveland, C.C. and Liptzin, D. (2007) C:N:P stoichiometry in soil: is there a “Redfield ratio”
883 for the microbial biomass? *Biogeochemistry* 85, 235-252.

884 del Giorgio, P.A. and Cole, J.J. (1998) Bacterial growth efficiency in natural aquatic systems.
885 *Annual Review of Ecology and Systematics* 29, 503-541.

886 Droop, M.R. (1974) The nutrient status of algal cells in continuous culture. *Journal of the Marine*
887 *Biological Association of the United Kingdom* 54, 825-855.

888 Druhan, J.L., Bill, M., Lim, H., Wu, C., Conrad, M.E., Williams, K.H., DePaolo, D.J. and
889 Brodie, E.L. (2014) A large column analog experiment of stable isotope variations during
890 reactive transport: II. Carbon mass balance, microbial community structure and
891 predation. *Geochimica et Cosmochimica Acta* 124, 394-409.

892 Druhan, J.L., Steefel, C.I., Molins, S., Williams, K.H., Conrad, M.E. and DePaolo, D.J. (2012)
893 Timing the onset of sulfate reduction over multiple subsurface acetate amendments by
894 measurement and modeling of sulfur isotope fractionation. *Environmental Science and*
895 *Technology* 46, 8895-8902.

896 Edwards, J.S., Ramakrishna, R., Schilling, C.H. and Palsson, B.O. (1999) Metabolic Flux
897 Balance Analysis, In: *Metabolic Engineering* Edited by Lee SY, Papoutsakis ET. pp. 13-
898 57: Marcel Dekker;

899 Egli, T. (2013) The ecological and physiological significance of the growth of heterotrophic.
900 Advances in Microbial Ecology 14, 305-386.

901 Elser, J.J., Bracken, M.E.S., Cleland, E.E., Gruner, D.S., Harpole, W.S., Hillebrand, H., Ngai,
902 J.T., Seabloom, E.W., Shurin, J.B. and Smith, J.E. (2007) Global analysis of nitrogen and
903 phosphorus limitation of primary producers in freshwater, marine and terrestrial
904 ecosystems. Ecology Letters 10, 1135-1142.

905 Fang, Y., Scheibe, T.D., Mahadevan, R., Garg, S., Long, P.E. and Lovley, D.R. (2011) Direct
906 coupling of a genome-scale microbial *in silico* model and a groundwater reactive
907 transport model. Journal of Contaminant Hydrology 122, 96-103.

908 Fang, Y., Yabusaki, S.B., Morrison, S.J., Amonette, J.P. and Long, P.E. (2009) Multicomponent
909 reactive transport modeling of uranium bioremediation field experiments. Geochimica et
910 Cosmochimica Acta 73, 6029-6051.

911 Feist, A.M. and Palsson, B.O. (2008) The growing scope of applications of genome-scale
912 metabolic reconstructions using *Escherichia coli*. Nat Biotech 26, 659-667.

913 Feist, A.M. and Palsson, B.O. (2010) The biomass objective function. Current Opinion in
914 Microbiology 13, 344-349.

915 Feist, A.M., Scholten, J.C.M., Palsson, B.O., Brockman, F.J. and Ideker, T. (2006) Modeling
916 methanogenesis with a genome-scale metabolic reconstruction of *Methanosarcina*
917 *barkeri*. Mol Syst Biol 2.

918 Ferry, J.G. (2010) Biochemistry of acetotrophic methanogenesis, in: McGenity, T.J., McGenity,
919 T., Meer, J.R.v.d., Lorenzo, V.d. (Eds.), Handbook of Hydrocarbon and Lipid
920 Microbiology. Springer Berlin Heidelberg, pp. 357-367.

921 Fukuzaki, S., Nishio, N. and Nagai, S. (1990) Kinetics of the methanogenic fermentation of
922 acetate. Applied and Environmental Microbiology 56, 3158-3163.

923 Gonnerman, M.C., Benedict, M.N., Feist, A.M., Metcalf, W.W. and Price, N.D. (2013)
924 Genomically and biochemically accurate metabolic reconstruction of *Methanosarcina*
925 *barkeri* Fusaro, iMG746. Biotechnology journal 8, 1070-1079.

926 Hedderich, R. and Whitman, W. (2006) Physiology and biochemistry of the methane-producing
927 archaea, in: Dworkin, M., Falkow, S., Schleifer, K.-H., Rosenberg, E., Stackebrandt, E.
928 (Eds.), The Prokaryotes. Springer, Singapore, pp. 1050-1079.

929 Henson, M.A. and Hanly, T.J. (2014) Dynamic flux balance analysis for synthetic microbial

930 communities, IET Systems Biology. Institution of Engineering and Technology, pp. 214-
931 229.

932 Herrgård, M.J., Lee, B.-S., Portnoy, V. and Palsson, B.Ø. (2006) Integrated analysis of
933 regulatory and metabolic networks reveals novel regulatory mechanisms in
934 *Saccharomyces cerevisiae*. *Genome Research* 16, 627-635.

935 Hespell, R.B. and Bryant, M.P. (1979) Efficiency of rumen microbial growth: Influence of some
936 theoretical and experimental factors on Y_{ATP} . *Journal of Animal Science* 49, 1640-1659.

937 Hoehler, T.M. and Jørgensen, B.B. (2013) Microbial life under extreme energy limitation.
938 *Nature Reviews Microbiology* 11, 83-94.

939 Jablonski, P.E. and Ferry, J.G. (1991) Purification and properties of methyl coenzyme M
940 methylreductase from acetate-grown *Methanosarcina thermophila*. *Journal of*
941 *Bacteriology* 173, 2481-2487.

942 Jannasch, H.W. (1967) Growth of marine bacteria at limiting concentrations of organic carbon in
943 seawater. *Limnology and Oceanography* 12, 264-271.

944 Jin, Q. (2012) Energy conservation of anaerobic respiration. *American Journal of Science* 312,
945 573-628.

946 Jin, Q. and Bethke, C.M. (2002) Kinetics of electron transfer through the respiratory chain.
947 *Biophysical Journal* 83, 1797-1808.

948 Jin, Q. and Bethke, C.M. (2003) A new rate law describing microbial respiration. *Applied and*
949 *Environmental Microbiology* 69, 2340-2348.

950 Jin, Q. and Bethke, C.M. (2005) Predicting the rate of microbial respiration in geochemical
951 environments. *Geochimica et Cosmochimica Acta* 69, 1133-1143.

952 Jin, Q. and Bethke, C.M. (2007) The thermodynamics and kinetics of microbial metabolism.
953 *American Journal of Science* 307, 643-677.

954 Jin, Q. and Bethke, C.M. (2009) Cellular energy conservation and the rate of microbial sulfate
955 reduction. *Geology* 36, 739-742.

956 Jin, Q. and Roden, E.E. (2011) Microbial physiology-based model of ethanol metabolism in
957 subsurface sediments. *Journal of Contaminant Hydrology* 125, 1-12.

958 Jin, Q., Roden, E.E. and Giska, J.R. (2013) Geomicrobial kinetics: extrapolating laboratory
959 studies to natural environments. *Geomicrobiology Journal* 30, 173-185.

960 Johannesson, K.H. and Neumann, K. (2012) Geochemical cycling of mercury in a deep, confined

961 aquifer: Insights from biogeochemical reactive transport modeling. *Geochimica et*
962 *Cosmochimica Acta*.

963 Kadam, P.C. and Boone, D.R. (1996) Influence of pH on Ammonia Accumulation and Toxicity
964 in Halophilic, Methylotrophic Methanogens. *Applied and Environmental Microbiology*
965 62, 4486-4492.

966 Keller, J.K. and Bridgham, S.D. (2007) Pathways of anaerobic carbon cycling across an
967 ombrotrophic-minerotrophic peatland gradient. *Limnology and Oceanography* 52, 96-
968 107.

969 Kenealy, W.R., Thompson, T.E., Schubert, K.R. and Zeikus, J.G. (1982) Ammonia assimilation
970 and synthesis of alanine, aspartate, and glutamate in *Methanosarcina barkeri* and
971 *Methanobacterium thermoautotrophicum*. *Journal of Bacteriology* 150, 1357-1365.

972 Kessler, P.S., Daniel, C. and Leigh, J.A. (2001) Ammonia Switch-Off of Nitrogen Fixation in the
973 Methanogenic Archaeon *Methanococcus maripaludis*: Mechanistic Features and
974 Requirement for the Novel GlnB Homologues, NifI1 and NifI2. *Journal of Bacteriology*
975 183, 882-889.

976 Klier, C. (2012) Use of an uncertainty analysis for genome-scale models as a prediction tool for
977 microbial growth processes in subsurface environments. *Environmental Science &*
978 *Technology* 46, 2790-2798.

979 Kliphuis, A.M.J., Klok, A.J., Martens, D.E., Lamers, P.P., Janssen, M. and Wijffels, R.H. (2012)
980 Metabolic modeling of *Chlamydomonas reinhardtii*: energy requirements for
981 photoautotrophic growth and maintenance. *Journal of Applied Phycology* 24, 253-266.

982 Knelman, J.E., Schmidt, S.K., Lynch, R.C., Darcy, J.L., Castle, S.C., Cleveland, C.C. and
983 Nemergut, D.R. (2014) Nutrient Addition Dramatically Accelerates Microbial
984 Community Succession. *PLOS ONE* 9, e102609.

985 Komlos, J., Peacock, A., Kukkadapu, R.K. and Jaffé, P.R. (2008) Long-term dynamics of
986 uranium reduction/reoxidation under low sulfate conditions. *Geochimica et*
987 *Cosmochimica Acta* 72, 3603-3615.

988 Krzycki, J.A., Wolkin, R.H. and Zeikus, J.G. (1982) Comparison of unitrophic and mixotrophic
989 substrate metabolism by an acetate-adapted strain of *Methanosarcina barkeri*. *Journal of*
990 *Bacteriology* 149, 247-254.

991 LeBauer, D.S. and Treseder, K.K. (2008) NITROGEN LIMITATION OF NET PRIMARY

992 PRODUCTIVITY IN TERRESTRIAL ECOSYSTEMS IS GLOBALLY
993 DISTRIBUTED. *Ecology* 89, 371-379.

994 Li, L., Steefel, C.I., Williams, K.H., Wilkins, M.J. and Hubbard, S.S. (2009) Mineral
995 transformation and biomass accumulation associated with uranium bioremediation at
996 Rifle, Colorado. *Environmental Science and Technology* 43, 5429-5435.

997 Liang, Y., Van Nostrand, J.D., N'Guessan, L.A., Peacock, A.D., Deng, Y., Long, P.E., Resch,
998 C.T., Wu, L., He, Z., Li, G., Hazen, T.C., Lovley, D.R. and Zhou, J. (2012) Microbial
999 Functional Gene Diversity with a Shift of Subsurface Redox Conditions during In Situ
1000 Uranium Reduction. *Applied and Environmental Microbiology* 78, 2966-2972.

1001 Ma, K. and Thauer, R.K. (1990) N5, N10-Methylenetetrahydromethanopterin reductase from
1002 *Methanosarcina barkeri*. *FEMS Microbiology Letters* 70, 119-123.

1003 Mah, R.A., Smith, M.R. and Baresi, L. (1978) Studies on an acetate-fermenting strain of
1004 *Methanosarcina*. *Applied and Environmental Microbiology* 35, 1174-1184.

1005 Mahadevan, R., Edwards, J.S. and Doyle Iii, F.J. (2002) Dynamic flux balance analysis of
1006 diauxic growth in *Escherichia coli*. *Biophys J* 83.

1007 Mahadevan, R., Palsson, B.Ø. and Lovley, D.R. (2011) *In situ* to *in silico* and back: elucidating
1008 the physiology and ecology of *Geobacter* spp. using genome-scale modelling. *Nature*
1009 *Reviews Microbiology* 9, 39-50.

1010 Majone, M., Verdini, R., Aulenta, F., Rossetti, S., Tandoi, V., Kalogerakis, N., Agathos, S., Puig,
1011 S., Zanaroli, G. and Fava, F. (2015) In situ groundwater and sediment bioremediation:
1012 barriers and perspectives at European contaminated sites. *New Biotechnology* 32, 133-
1013 146.

1014 Mazumder, T.K., Nishio, N., Fukuzaki, S. and Nagai, S. (1986) Effect of sulfur-containing
1015 compounds on growth of *Methanosarcina barkeri* in defined medium. *Applied and*
1016 *Environmental Microbiology* 52, 617-622.

1017 McMahon, P.B. and Chapelle, F.H. (1991a) Geochemistry of dissolved inorganic carbon in a
1018 Coastal Plain aquifer. 2. Modeling carbon sources, sinks, and $\delta^{13}\text{C}$ evolution. *Journal of*
1019 *Hydrology* 127, 109-135.

1020 McMahon, P.B. and Chapelle, F.H. (1991b) Microbial production of organic acids in aquitard
1021 sediments and its role in aquifer geochemistry. *Nature* 349, 233-235.

1022 Meadows, A.L., Karnik, R., Lam, H., Forestell, S. and Snedecor, B. (2010) Application of

1023 dynamic flux balance analysis to an industrial *Escherichia coli* fermentation. *Metabolic*
1024 *Engineering* 12, 150-160.

1025 MeGee, R.D.I., Drake, J.F., Fredrickson, A.G. and Tsuchiya, H.M. (1972) Studies in
1026 intermicrobial symbiosis. *Saccharomyces cerevisiae* and *Lactobacillus casei*. *Canadian*
1027 *Journal of Microbiology* 18, 1733-1742.

1028 Mitchell, D.A., von Meien, O.F., Krieger, N. and Dalsenter, F.D.H. (2004) A review of recent
1029 developments in modeling of microbial growth kinetics and intraparticle phenomena in
1030 solid-state fermentation. *Biochemical Engineering Journal* 17, 15-26.

1031 Monod, J. (1949) The growth of bacterial cultures. *Annual Review of Microbiology* 3, 371-394.

1032 Moran, J.J., House, C.H., Vrentas, J.M. and Freeman, K.H. (2008) Methyl Sulfide Production by
1033 a Novel Carbon Monoxide Metabolism in *Methanosarcina acetivorans*. *Applied and*
1034 *Environmental Microbiology* 74, 540-542.

1035 Morita, R.Y. (1997) Bacteria in Oligotrophic Environments. Chapman & Hall, New York.

1036 Mouser, P.J., N'Guessan, A.L., Elifantz, H., Holmes, D.E., Williams, K.H., Wilkins, M.J., Long,
1037 P.E. and Lovley, D.R. (2009) Influence of Heterogeneous Ammonium Availability on
1038 Bacterial Community Structure and the Expression of Nitrogen Fixation and Ammonium
1039 Transporter Genes during in Situ Bioremediation of Uranium-Contaminated
1040 Groundwater. *Environmental Science & Technology* 43, 4386-4392.

1041 Murphy, E.M. and Schramke, J.A. (1998) Estimation of microbial respiration rates in
1042 groundwater by geochemical modeling constrained with stable isotopes. *Geochimica et*
1043 *Cosmochimica Acta* 62, 3395-3406.

1044 Nielsen, U.N., Ayres, E., Wall, D.H. and Bardgett, R.D. (2011) Soil biodiversity and carbon
1045 cycling: a review and synthesis of studies examining diversity–function relationships.
1046 *European Journal of Soil Science* 62, 105-116.

1047 Nisbet, E.G., Dlugokencky, E.J., Manning, M.R., Lowry, D., Fisher, R.E., France, J.L., Michel,
1048 S.E., Miller, J.B., White, J.W.C., Vaughn, B., Bousquet, P., Pyle, J.A., Warwick, N.J.,
1049 Cain, M., Brownlow, R., Zazzeri, G., Lanoisellé, M., Manning, A.C., Gloor, E., Worthy,
1050 D.E.J., Brunke, E.-G., Labuschagne, C., Wolff, E.W. and Ganesan, A.L. (2016) Rising
1051 atmospheric methane: 2007–2014 growth and isotopic shift. *Global Biogeochemical*
1052 *Cycles* 30, 1356-1370.

1053 Orth, J.D., Thiele, I. and Palsson, B.Ø. (2010) What is flux balance analysis? *Nature*

1054 biotechnology 28, 245-248.

1055 Peinemann, S., Muller, V., Blaut, M. and Gottschalk, G. (1988) Bioenergetics of methanogenesis
1056 from acetate by *Methanosarcina barkeri*. Journal of Bacteriology 170, 1369-1372.

1057 Phelps, T.J., Murphy, E.M., Pfiffner, S.M. and White, D.C. (1994a) Comparison between
1058 geochemical and biological estimates of subsurface microbial activities. Microbial
1059 Ecology 28, 335-349.

1060 Phelps, T.J., Pfiffner, S.M., Sargent, K.A. and White, D.C. (1994b) Factors influencing the
1061 abundance and metabolic capacities of microorganisms in Eastern Coastal Plain
1062 sediments. Microbial Ecology 28, 351-364.

1063 Price, P.B. and Sowers, T. (2004) Temperature dependence of metabolic rates for microbial
1064 growth, maintenance, and survival. Proceedings of the National Academy of Sciences
1065 101, 4631-4636.

1066 Reed, J.L. and Palsson, B.Ø. (2003) Thirteen years of building constraint-based *in silico* models
1067 of *Escherichia coli*. Journal of Bacteriology 185, 2692-2699.

1068 Rittmann, B.E. and McCarty, P.L. (2012) Environmental biotechnology: principles and
1069 applications. Tata McGraw-Hill Education.

1070 Roden, E.E. and Jin, Q. (2011) Thermodynamics of microbial growth coupled to metabolism of
1071 glucose, ethanol, short-chain organic acids, and hydrogen. Applied and Environmental
1072 Microbiology 77, 1907-1909.

1073 Roszak, D.B. and Colwell, R.R. (1987) Survival strategies of bacteria in the natural environment.
1074 Microbiological Reviews 51, 365-379.

1075 Russell, J.B. and Cook, G.M. (1995) Energetics of bacterial growth: balance of anabolic and
1076 catabolic reactions. Microbiological Reviews 59, 48-62.

1077 Scheibe, T.D., Mahadevan, R., Fang, Y., Garg, S., Long, P.E. and Lovley, D.R. (2009) Coupling
1078 a genome-scale metabolic model with a reactive transport model to describe *in situ*
1079 uranium bioremediation. Microbial Biotechnology 2, 274-286.

1080 Schellenberger, J., Que, R., Fleming, R.M.T., Thiele, I., Orth, J.D., Feist, A.M., Zielinski, D.C.,
1081 Bordbar, A., Lewis, N.E., Rahmanian, S., Kang, J., Hyduke, D.R. and Palsson, B.O.
1082 (2011) Quantitative prediction of cellular metabolism with constraint-based models: the
1083 COBRA Toolbox v2.0. Nat. Protocols 6, 1290-1307.

1084 Scherer, P. and Sahm, H. (1981) Influence of sulphur-containing compounds on the growth of

1085 <i>Methanosa^rcina barkeri in a defined medium. Applied Microbiology and
1086 Biotechnology 12, 28-35.

1087 Schimel, J. and Schaeffer, S. (2012) Microbial control over carbon cycling in soil. Frontiers in
1088 Microbiology 3.

1089 Schmidt, S.K. (1992) Models for studying the population ecology of microorganisms in natural
1090 systems, in: Hurst, C.J. (Ed.), Modeling the Metabolic and Physiologic Activities of
1091 Microorganisms. John Wiley & Sons Inc, pp. 31-59.

1092 Simkins, S. and Alexander, M. (1984) Models for mineralization kinetics with the variables of
1093 substrate concentration and population density. Applied and Environmental Microbiology
1094 47, 1299-1306.

1095 Sinsabaugh, R.L., Manzoni, S., Moorhead, D.L. and Richter, A. (2013) Carbon use efficiency of
1096 microbial communities: stoichiometry, methodology and modelling. Ecology Letters 16,
1097 930-939.

1098 Smith, M.R. and Mah, R.A. (1978) Growth and methanogenesis by *Methanosa^rcina* strain 227
1099 on acetate and methanol. Applied and Environmental Microbiology 36, 870-879.

1100 Smith, M.W., Davis, R.E., Youngblut, N.D., Kärnä, T., Herfort, L., Whitaker, R.J., Metcalf,
1101 W.W., Tebo, B.M., Baptista, A.M. and Simon, H.M. (2015) Metagenomic evidence for
1102 reciprocal particle exchange between the mainstem estuary and lateral bay sediments of
1103 the lower Columbia River. Frontiers in Microbiology 6.

1104 Sowers, K.R., Nelson, M.J. and Ferry, J.G. (1984) Growth of acetotrophic, methane-producing
1105 bacteria in a pH auxostat. Current Microbiology 11, 227-229.

1106 Stefano, M., Philip, T., Andreas, R., Amilcare, P. and I., Å.G. (2012) Environmental and
1107 stoichiometric controls on microbial carbon-use efficiency in soils. New Phytologist 196,
1108 79-91.

1109 Stolyar, S., Van Dien, S., Hillesland, K.L., Pinel, N., Lie, T.J., Leigh, J.A. and Stahl, D.A. (2007)
1110 Metabolic modeling of a mutualistic microbial community. Molecular systems biology 3,
1111 n/a-n/a.

1112 Tanford, C. (1983) Mechanism of Free Energy Coupling in Active Transport. Annual Review of
1113 Biochemistry 52, 379-409.

1114 Tartakovsky, G.D., Tartakovsky, A.M., Scheibe, T.D., Fang, Y., Mahadevan, R. and Lovley,
1115 D.R. (2013) Pore-scale simulation of microbial growth using a genome-scale metabolic

1116 model: Implications for Darcy-scale reactive transport. *Advances in Water Resources* 59,
1117 256-270.

1118 Tempest, D.W. and Neijssel, O.M. (1984) The status of Y_{ATP} and maintenance energy as
1119 biologically interpretable phenomena. *Annual Review of Microbiology* 38, 459-486.

1120 Thauer, R.K., Kaster, A.-K., Seedorf, H., Buckel, W. and Hedderich, R. (2008) Methanogenic
1121 archaea: ecologically relevant differences in energy conservation. *Nature Reviews
1122 Microbiology* 6, 579-591.

1123 Thiele, I. and Palsson, B.Ø. (2010) A protocol for generating a high-quality genome-scale
1124 metabolic reconstruction. *Nature protocols* 5, 93-121.

1125 van Bodegom, P. (2007) Microbial maintenance: A critical review on its quantification.
1126 *Microbial Ecology* 53, 513-523.

1127 Vargas, F.A., Pizarro, F., Pérez-Correa, J.R. and Agosin, E. (2011) Expanding a dynamic flux
1128 balance model of yeast fermentation to genome-scale. *BMC Systems Biology* 5, 75.

1129 Wandrey, C. and Aivasidis, A. (1983) Continuous anaerobic digestion with *Methanosarcina*
1130 *barkeri*. *Annals of the New York Academy of Sciences* 413, 489-500.

1131 Welte, C. and Deppenmeier, U. (2013) Bioenergetics and anaerobic respiratory chains of
1132 aceticlastic methanogens. *Biochimica et Biophysica Acta (BBA)-Bioenergetics*.

1133 Welte, C., Kröninger, L. and Deppenmeier, U. (2014) Experimental evidence of an acetate
1134 transporter protein and characterization of acetate activation in aceticlastic
1135 methanogenesis of *Methanosarcina mazei*. *FEMS Microbiology Letters* 359, 147-153.

1136 Westermann, P., Ahring, B.K. and Mah, R.A. (1989) Threshold acetate concentrations for
1137 acetate catabolism by aceticlastic methanogenic bacteria. *Applied and Environmental
1138 Microbiology* 55, 514-515.

1139 Whitman, W., Bowen, T. and Boone, D. (2006) The Methanogenic Bacteria, in: Dworkin, M.,
1140 Falkow, S., Schleifer, K.-H., Rosenberg, E., Stackebrandt, E. (Eds.), *The Prokaryotes*.
1141 Springer Singapore, pp. 165-207.

1142 Winternute, E.H., Lieberman, T.D. and Silver, P.A. (2013) An objective function exploiting
1143 suboptimal solutions in metabolic networks. *BMC Systems Biology* 7, 98.

1144 Yabusaki, S.B., Fang, Y., Williams, K.H., Murray, C.J., Ward, A.L., Dayvault, R.D., Waichler,
1145 S.R., Newcomer, D.R., Spane, F.A. and Long, P.E. (2011) Varily saturated flow and
1146 multicomponent biogeochemical reactive transport modeling of a uranium

1147 bioremediation field experiment. *Journal of Contaminant Hydrology* 126, 271-290.

1148 Yang, S.T. and Okos, M.R. (1987) Kinetic study and mathematical modeling of methanogenesis

1149 of acetate using pure cultures of methanogens. *Biotechnology and Bioengineering* 30,

1150 661-667.

1151 Ye, R., Jin, Q., Bohannan, B., Keller, J.K., McAllister, S.A. and Bridgman, S.D. (2012) pH

1152 controls over anaerobic carbon mineralization, the efficiency of methane production, and

1153 methanogenic pathways in peatlands across an ombrotrophic–minerotrophic gradient.

1154 *Soil Biology and Biochemistry* 54, 36-47.

1155 Zhang, G., Jiang, N., Liu, X. and Dong, X. (2008) Methanogenesis from Methanol at Low

1156 Temperatures by a Novel Psychrophilic Methanogen, “*Methanolobus psychrophilus*” sp.

1157 nov., Prevalent in Zoige Wetland of the Tibetan Plateau. *Applied and Environmental*

1158 *Microbiology* 74, 6114-6120.

1159 Zhao, J., Scheibe, T.D. and Mahadevan, R. (2011) Model-based analysis of the role of

1160 biological, hydrological and geochemical factors affecting uranium bioremediation.

1161 *Biotechnology and Bioengineering* 108, 1537-1548.

1162 Zhou, L., Yu, H., Ai, G., Zhang, B., Hu, S. and Dong, X. (2015) Transcriptomic and

1163 Physiological Insights into the Robustness of Long Filamentous Cells of *Methanosaeta*

1164 *harundinacea*, Prevalent in Upflow Anaerobic Sludge Blanket Granules. *Applied and*

1165 *Environmental Microbiology* 81, 831-839.

1166 Zhuang, K., Izallalen, M., Mouser, P., Richter, H., Risso, C., Mahadevan, R. and Lovley, D.R.

1167 (2010) Genome-scale dynamic modeling of the competition between *Rhodoferax* and

1168 *Geobacter* in anoxic subsurface environments. *The ISME Journal* 5, 305-316.

1169 Zinn, M., Witholt, B. and Egli, T. (2004) Dual nutrient limited growth: models, experimental

1170 observations, and applications. *Journal of Biotechnology* 113, 263-279.

1171 Zwietering, M.H., Jongenburger, I., Rombouts, F.M. and van 't Riet, K. (1990) Modeling of the

1172 Bacterial Growth Curve. *Applied and Environmental Microbiology* 56, 1875-1881.

1173

1174 Table 1. Parameters and their values for applying different modeling methods to *Methanosaarcina barkeri* growing on acetate.

Parameter ^(a)	Value	Rate law	dynamic FBA	Hybrid method
<u>Respiration parameter</u>				
Rate constant k (mmol·g ⁻¹ ·hr ⁻¹)	7.1 ^(a,b)	✓		✓
half-saturation constant K_D (mM)	5.0 ^(b,c)	✓		✓
ATP yield ν_P	0 ~ 1 ^(d)	✓		
Phosphorylation energy ΔG_P (kJ·mol ⁻¹)	40 ^(d)	✓		✓
Average stoichiometric number χ	2 ^(a,e)	✓		✓
Proton motive force (V)	0.1 ^(d)			✓
<u>Growth parameters</u>				
Growth yield $Y_{X/R}$ (g·mol ⁻¹)	2.9 ^(d)	✓		
Maintenance rate m (hr ⁻¹)	1.8×10 ^{-4(f)}	✓	✓ ^(g)	✓
<u>Acetate uptake</u>				
Maximum rate V_{max} (mmol·g ⁻¹ ·hr ⁻¹)	2.2 ^(h)		✓	
Michaelis constant $K_{ac,out}$	0.3 ^(h)		✓	
<u>Ammonium uptake</u>				
Maximum rate V_{max} (mmol·g ⁻¹ ·hr ⁻¹)	0.25 ⁽ⁱ⁾		✓	

Michaelis constant for ammonium in the environment $K_{N,env}$ (μM)	$200^{(j)}$	✓	✓
Michaelis constant for cytoplasmic ammonium $K_{N,cyt}$ (μM)	$2000^{(k)}$		✓
Exponent n	$2^{(i)}$		✓
Total parameters		7	5
			9

1175

1176 Note:

1177 (a). Values expressed for reaction equation 16.

1178 (b). Smith and Mah (1978).

1179 (c). Acetate is accounted for as the electron donor in the modified Monod equation (eq 1).

1180 (d). Jin (2012).

1181 (e). Jin and Bethke (2009).

1182 (f). Wandrey and Aivasidis (1983).

1183 (g). In model iMG746, the hypothetical ATP hydrolysis reaction of maintenance has a rate of $2.0 \text{ mmol} \cdot \text{g}^{-1} \cdot \text{hr}^{-1}$ (Gonnerman et al., 2013).

1185 (h). Button (1998)

1186 (i). This study.

1187 (j). Boogerd et al. (2011).

1188 (k). Chang et al. (2014).

1189 **Figure Caption**

1190 Figure 1. Comparison of dynamic FBA (A) and the hybrid method of FBA and microbial rate
1191 law (B). Dynamic FBA calculates uptake fluxes of electron donors, acceptors, and nutrients
1192 using the Michaelis-Menten equation (eq 5), and applies FBA to entire genome-scale metabolic
1193 models. The hybrid method applies FBA to the respiration pathways to estimate ATP yields, and
1194 computes respiration rates and ATP fluxes using the thermodynamically-consistent Monod
1195 equation (eqs 1 and 12); it estimates nutrient uptake fluxes by optimizing cytoplasmic nutrient
1196 concentration (eq 10) and by using the thermodynamically-consistent Michaelis-Menten
1197 equation (eqs 7 and 8), and then applies FBA to the biosynthesis pathways using the fluxes of
1198 ATP production and nutrient uptake as the input.

1199

1200 Figure 2. Variations in cytoplasmic ammonium accumulation (A and B) and uptake (C) with
1201 ammonium concentrations in the environment. Panel A and B show ammonium accumulation in
1202 laboratory reactors and in natural environments, respectively. Data points in panel A are the
1203 laboratory observations of *Methanohalophilus zhilinaeae* (\diamond), *Methanolobus bombay* (\circ), and
1204 *Methanolobus taylorii* (\square) by Kadam and Boone (1996). The solid lines in panel A and B are the
1205 optimization results (eq 10). The solid line in panel C is computed according to the
1206 thermodynamically-consistent Michaelis-Menten equation (eqs 7 and 8) using the parameters in
1207 table 1, while the dashed line indicates the maximum ammonium uptake flux.

1208

1209 Figure 3. Variations in the concentrations of acetate, methane, and ammonium (A), and biomass
1210 (B), the fluxes of ATP production and acetate consumption by methanogenesis (C), the fluxes of
1211 acetate and ammonium consumption by biosynthesis (D), growth rate (E), and the energy ΔG_A

1212 available from methanogenesis (F) during the growth of *M. barkeri* on acetate. Data points are
1213 the experimental results of Fukuzaki et al. (1990); solid lines are the simulation results of the
1214 hybrid method; the dashed lines in panel A and B are the result of dynamic FBA. The dotted line
1215 in panel D shows the maximum possible uptake flux of ammonium, and the dotted line in panel
1216 F shows the energy ΔG_C conserved by methanogenesis (eq 11). The lines labeled “FBA
1217 infeasible” in panel A and B indicate the time point beyond which ATP synthesis rate by
1218 methanogenesis is smaller than ATP consumption rate by maintenance assumed in model
1219 iMG746, and dynamic FBA fails to find a solution.

1220

1221 Figure 4. Variations with acetate concentration in biosynthesis rate and generation time (A) and
1222 biomass yield (C) at 10 μM and at other ammonium concentrations (B and D), and changes in
1223 carbon use efficiency (CUE) with the atomic ratios of C in acetate and N in ammonium at 10 μM
1224 (E) and at other ammonium concentrations (F). The solid lines are the predictions of the hybrid
1225 method by taking temperature at 25 $^{\circ}\text{C}$, pH at 7, and bicarbonate concentration at 1 mM; the
1226 dashed lines in panel A and B are the maximum biosynthesis rates at given ammonium
1227 concentrations; the dashed lines in C and D are the maximum and minimum biomass yields; the
1228 dashed lines in E and F are the maximum and minimum CUEs; labels in panel A, C, and E show
1229 the methane concentrations in μM ; labels in panel B, D, and F show ammonium concentrations
1230 in μM . The generation time is computed as the ratio of $\ln(2)$ to specific biosynthesis rate.
1231 Biomass yields and CUEs are calculated according to equation 19 and 20, respectively.

1232

1233 Figure 5. The correlation between ammonium and methane concentrations in the siliciclastic
1234 aquifers of Pennsylvania, USA.

1235

1236 Figure 6. Variations with time in the ATP fluxes (O) from methanogenesis (A to D), the
1237 ammonium uptake fluxes (●, E to H), the growth rates predicted by the hybrid method (▲) and
1238 by the linear equation (eqs 2 and 3, Δ, I to L), the carbon use efficiencies (CUEs, M to P),
1239 groundwater ammonium concentrations (■), and the ammonium concentrations (□) required to
1240 support the stoichiometrically-balanced biosynthesis of methanogens (Q to T) in the groundwater
1241 from wells D-02, D-04, D-05, and D-08 during the field bioremediation experiments (Mouser et
1242 al., 2009). The dotted lines in panel I to L indicate no growth.

1243

1244 Figure 7. Variations in the expression of ammonium transporters with the ratio of ammonium
1245 concentration m_{env} in the environment to the concentration m_{req} required to support the
1246 stoichiometrically-balanced biosynthesis of *M. barkeri*. The expression is measured as the ratio
1247 in mRNA transcript copy of an ammonium transporter gene *amtB* to a housekeeping gene *recA*
1248 gene in groundwater samples from well D-02 (O), 04 (□), 05 (◊), and 08 (▲) by Mouser et al.
1249 (2009, their figure S4); the shaded area indicates that ammonium in the environment cannot meet
1250 the requirement of biosynthesis, and hence is limiting growth.

1251